



UNIVERSITY OF LEEDS

This is a repository copy of *Chaos in magnetoconvection*.

White Rose Research Online URL for this paper:

<http://eprints.whiterose.ac.uk/979/>

Article:

Rucklidge, A.M. (1994) Chaos in magnetoconvection. *Nonlinearity*, 7 (6). 1565 -1591. ISSN 1361-6544

<https://doi.org/10.1088/0951-7715/7/6/003>

Reuse

Unless indicated otherwise, fulltext items are protected by copyright with all rights reserved. The copyright exception in section 29 of the Copyright, Designs and Patents Act 1988 allows the making of a single copy solely for the purpose of non-commercial research or private study within the limits of fair dealing. The publisher or other rights-holder may allow further reproduction and re-use of this version - refer to the White Rose Research Online record for this item. Where records identify the publisher as the copyright holder, users can verify any specific terms of use on the publisher's website.

Takedown

If you consider content in White Rose Research Online to be in breach of UK law, please notify us by emailing eprints@whiterose.ac.uk including the URL of the record and the reason for the withdrawal request.



eprints@whiterose.ac.uk
<https://eprints.whiterose.ac.uk/>



White Rose
university consortium
Universities of Leeds, Sheffield & York

White Rose Consortium ePrints Repository

<http://eprints.whiterose.ac.uk/>

This is an author produced version of a paper published in **Nonlinearity**. This paper has been peer-reviewed but does not include final publisher proof-corrections or journal pagination.

White Rose Repository URL for this paper:
<http://eprints.whiterose.ac.uk/archive/00000979/>

Citation for the published paper

Rucklidge, A.M. (1994) *Chaos in magnetoconvection*. *Nonlinearity*, 7 (6). 1565 - 1591.

Citation for this paper

To refer to the repository paper, the following format may be used:

Rucklidge, A.M. (1994) *Chaos in magnetoconvection*. Author manuscript available at:

<http://eprints.whiterose.ac.uk/archive/00000979/> [Accessed: *date*].

Published in final edited form as:

Rucklidge, A.M. (1994) *Chaos in magnetoconvection*. *Nonlinearity*, 7 (6). 1565 - 1591.

Chaos in magnetoconvection

A M Rucklidge

Department of Applied Mathematics and Theoretical Physics,
University of Cambridge, Cambridge CB3 9EW, UK

Abstract. The partial differential equations (PDEs) for two-dimensional incompressible convection in a strong vertical magnetic field have a codimension-three bifurcation when the parameters are chosen so that the bifurcations to steady and oscillatory convection coincide and the limit of narrow rolls is taken. The third-order set of ordinary differential equations (ODEs) that govern the behaviour of the PDEs near this bifurcation are derived using perturbation theory. These ODEs are the normal form of the codimension-three bifurcation; as such, they prove to be an excellent predictor of the behaviour of the PDEs. This is the first time that a detailed comparison has been made between the chaotic behaviour of a set of PDEs and that of the corresponding set of model ODEs, in a parameter regime where the ODEs are expected to provide accurate approximations to solutions of the PDEs. Most significantly, the transition from periodic orbits to a chaotic Lorenz attractor predicted by the ODEs is recovered in the PDEs, making this one of the few situations in which the nature of chaotic oscillations observed numerically in PDEs can be established firmly. Including correction terms obtained from the perturbation calculation enables the ODEs to track accurately the bifurcations in the PDEs over an appreciable range of parameter values. Numerical calculations suggest that the T-point (where there are heteroclinic connections between a saddle point and a pair of saddle-foci), which is associated with the transition from a Lorenz attractor to a quasi-attractor in the normal form, is also found in the PDEs. Further numerical simulations of the PDEs with square rolls confirm the existence of chaotic oscillations associated with a heteroclinic connection between a pair of saddle-foci.

1. Introduction

It is not often that it is possible to establish analytically the nature of chaotic solutions observed numerically in partial differential equations (PDEs). Rucklidge (1992, 1993) showed how the PDEs for two-dimensional Boussinesq convection in a vertical magnetic field could be reduced, for a particular range of parameters, first to a third-order set of ordinary differential equations (ODEs), and then to a one-dimensional map. The analysis of the map shows an abrupt transition from periodic to chaotic behaviour. In this paper, we present systematic and accurate numerical solutions of the same PDEs and compare them with the predictions of the third-order model and the one-dimensional map, demonstrating a remarkably good quantitative agreement between the chaotic behaviour of the map, the PDEs and the corresponding set of model ODEs. The main points of this paper are twofold: first, this is the first time that apparently chaotic numerical solutions of a set of PDEs can genuinely be demonstrated to be chaotic, and second, low-order models constructed by centre manifold or by perturbation techniques can (and do in this case) provide a quantitative description of the PDE behaviour over an appreciable range of parameter values.

In other studies, low-order models of the behaviour of sets of PDEs are often derived by a truncation procedure, perhaps the best-known example being the Lorenz (1963) equations. This celebrated third-order set of ODEs was first derived for Bénard convection in rolls, and its chaotic solutions aroused much interest. The Lorenz system correctly describes the transition to steady convection, but its chaotic solutions do not appear in the PDEs (Moore & Weiss 1973). In other cases, there is qualitative agreement between the chaotic behaviour of PDEs and truncated ODE models (for example, Knobloch *et al* 1986), but one cannot tell *a priori* whether or not the intricate behaviour observed in a truncated model will carry over to the PDEs from which it was derived. The approach adopted in this paper is to identify high-codimension bifurcation points where models constructed using the centre manifold technique will faithfully reproduce the behaviour of the PDEs arbitrarily well for parameters close enough to the bifurcation point. The numerical study of the PDEs presented here demonstrates that such carefully constructed models will also be a robust guide to the PDE behaviour even for parameter values not particularly close to the bifurcation point, and that the range of validity of the models can be extended by including higher-order terms. We focus on comparing two-parameter studies of the PDEs and the ODEs, rather than comparing the behaviour at single parameter values or along one-parameter slices.

Perturbation theory is used to reduce the PDEs to a third-order set of ODEs, but the choice of small parameters is inspired by centre manifold theory: the PDEs are expanded about a point that is known to have multiple zero eigenvalues. The first two zero eigenvalues are achieved by starting at a Takens–Bogdanov point, at which the pitchfork bifurcation to steady convection coincides with the Hopf bifurcation to oscillatory convection. Further zero eigenvalues are brought onto the centre manifold by considering the limit of narrow rolls: as L , the width of the rolls, goes to zero, the PDEs have eigenvalues that go to zero as $-L^2$, $-4L^2$, $-9L^2$ etc. A centre manifold calculation would include all corresponding eigenmodes (this would result in a PDE for the vertical structure), but the perturbation calculation reveals that only one mode is required, as all the others come in at higher order and can be ignored. The perturbation calculation also provides the $\mathcal{O}(L^2)$ corrections to the ODE model; including these dramatically improves the ability of the ODE model to make quantitative predictions of the locations of bifurcations over a wider range of parameter values.

That the model derived by perturbation theory from the PDEs should describe their behaviour so well is not surprising in the light of the recent calculations of Shil'nikov *et al* (1993), who showed that this third-order set of ODEs is the normal form of the particular codimension-three bifurcation that occurs in the PDEs at the Takens–Bogdanov point in the limit of narrow rolls. The normal forms for most codimension-one and two bifurcation have been analysed (Guckenheimer & Holmes 1983); the analysis of the normal forms of codimension-three bifurcations is complicated by the fact that such sets of ODEs often exhibit chaotic behaviour. However, the presence of this codimension-three bifurcation in a physical problem makes the effort of its analysis worthwhile.

The chaotic behaviour of the ODE model (and the PDEs) begins with the creation of a Lorenz attractor, which contains a countable infinity of unstable periodic orbits, an uncountable infinity of aperiodic trajectories and an orbit that is dense. Lorenz attractors are persistent over a range of parameter values, so the fact that one exists in the PDEs will not be affected by numerical errors or by the small terms discarded

from the ODE model. In subsequent bifurcations, there is a transition from a Lorenz attractor to a quasi-attractor (Shil'nikov 1993), a much more complicated object that can contain an infinite number of stable periodic orbits. Gonchenko *et al* (1993) proved that in a quasi-attractor, the details of the behaviour depend sensitively on the parameters in the problem, implying that it is pointless to continue the detailed comparison between the PDEs and the ODE model beyond the point of appearance of the quasi-attractor.

By considering the same limit of narrow rolls, Proctor & Weiss (1990) derived a fourth-order set of ODEs describing small-amplitude convection near the Takens–Bogdanov point for thermosolutal convection, and simplified the model to third-order in the limit of small solutal diffusivity. Their model equations have chaotic solutions associated with heteroclinic trajectories between saddle-foci, agreeing qualitatively with the numerical solutions of the PDEs for two-dimensional thermosolutal convection in rolls with aspect ratio of order one (Knobloch *et al* 1986). In a related study of triple convection (thermosolutal convection in a layer of fluid rotating about a vertical axis), Arnéodo *et al* (1982, 1985a), expanded about a codimension-three bifurcation point and obtained an asymptotically exact third-order model that has chaotic solutions, and that is in quantitative agreement with at least the steady behaviour of the PDEs (Arnéodo & Thual 1985).

The PDEs for two-dimensional Boussinesq convection in a vertical magnetic field are described in section 2; the derivation of the third-order model ODEs is in the Appendix, with the analysis of their bifurcation structure recalled in section 3. The numerical techniques used to solve the PDEs are outlined in section 4. The PDEs and the ODE model are compared for parameter values near the Takens–Bogdanov point in section 5, and in section 6, the development of chaotic solutions in the PDEs and ODEs as the roll width increases (up to the limit of validity of the ODE model) is described. We report numerical simulations of the PDEs in wider rolls in section 7, and discuss the origin of the chaotic solutions that were hinted at by Weiss (1981). We conclude in section 8.

2. Magnetoconvection in narrow rolls

The PDEs for two-dimensional convection in a Boussinesq fluid in the presence of a vertical magnetic field are (Proctor & Weiss 1982):

$$\nabla^2 \Psi = -\omega, \quad (2.1)$$

$$\frac{\partial \omega}{\partial t} + \mathbf{J}(\Psi, \omega) = \sigma \nabla^2 \omega - \sigma R \frac{\partial \theta}{\partial x} - \sigma \zeta Q \left(\frac{\partial \nabla^2 A}{\partial z} + \mathbf{J}(A, \nabla^2 A) \right), \quad (2.2)$$

$$\frac{\partial \theta}{\partial t} + \mathbf{J}(\Psi, \theta) = \nabla^2 \theta + \frac{\partial \Psi}{\partial x}, \quad (2.3)$$

$$\frac{\partial A}{\partial t} + \mathbf{J}(\Psi, A) = \zeta \nabla^2 A + \frac{\partial \Psi}{\partial z}, \quad (2.4)$$

where ω is the vorticity, Ψ is the stream-function with the velocity $\mathbf{u} = \nabla \times (\Psi \hat{\mathbf{y}})$, θ is the deviation from the static temperature profile so the temperature is $1 - z + \theta$, and A is the deviation from the uniform vertical magnetic field, so the total magnetic field is $\mathbf{B} = (-\partial A / \partial z, 0, 1 + \partial A / \partial x)$. The horizontal coordinate x and vertical coordinate z are scaled by the height h of the box. Time t is scaled by the thermal

diffusion time h^2/κ , where κ is the thermal diffusivity. The viscous Prandtl number $\sigma = \nu/\kappa$ and the magnetic diffusivity ratio $\zeta = \eta/\kappa$ (where ν and η are the viscous and magnetic diffusivities). Temperatures and magnetic fields are scaled by the temperature difference ΔT and the vertical magnetic field $\mathbf{B}_0 = B_0 \hat{\mathbf{z}}$ imposed across the box. The other parameters are the Rayleigh number

$$R = \frac{g\alpha h^3}{\kappa\nu} \Delta T, \quad (2.5)$$

and the Chandrasekhar number

$$Q = \frac{h^2}{\mu_0 \rho_0 \eta \nu} B_0^2, \quad (2.6)$$

where g is the acceleration due to gravity (acting in the negative z direction), α is the thermal expansion coefficient, ρ_0 is the reference density and μ_0 is the magnetic permeability of the fluid. The nonlinearities, contained in the Jacobian $J(f, g) = (\partial f/\partial x)(\partial g/\partial z) - (\partial f/\partial z)(\partial g/\partial x)$, represent the transport of vorticity, heat and magnetic flux; in addition, the fluid is driven by the nonlinear Lorentz force.

The fluid is confined to a box of fixed width L . It is convenient to adopt illustrative stress-free boundary conditions: $\omega = \Psi = 0$ on the boundary. The temperature is fixed at the top and bottom boundaries ($\theta = 0$ on $z = 0, 1$), with no heat flux across the sides ($\partial\theta/\partial x = 0$ on $x = 0, L$). The magnetic field is required to be vertical at the top and bottom boundaries ($\partial A/\partial z = 0$ on $z = 0, 1$) with no loss of magnetic flux across the sides ($A = 0$ on $x = 0, L$). Thus the five nondimensional parameters specifying the problem are σ , ζ , R , Q and the ‘aspect ratio’ $\varpi = 4L^2/(1 + L^2)$, with $0 \leq \varpi \leq 4$. Since σ and ζ will be fixed while ϖ will vary, it is useful to scale R and Q :

$$(R, Q) = \left(\frac{64\pi^4}{\varpi^2(4 - \varpi)} r, \frac{16\pi^2}{\varpi^2} q \right). \quad (2.7)$$

Two-dimensional Boussinesq magnetoconvection has been reviewed by Proctor & Weiss (1982; see also Weiss 1991 and Proctor 1992). If the temperature difference across the layer is small, then all fluid motion will decay due to viscous damping, leaving a uniform vertical magnetic field and a linear vertical temperature gradient. If the magnetic field is small, then the initial bifurcation as r increases is a pitchfork bifurcation from this state of no motion (the trivial solution) to one of steady convection. The two nontrivial steady solutions (one with the roll turning clockwise and the other with the roll turning counter-clockwise) are related by the reflection symmetry of the problem. As q increases, the tension in the magnetic lines of force opposes the convective motion, until q exceeds a critical value q_C , beyond which the initial bifurcation is a Hopf (oscillatory) bifurcation. At the bifurcation point C, where

$$(r, q) = (r_C, q_C) = \left(\frac{\sigma + \zeta}{\sigma(1 - \zeta)}, \frac{\zeta(1 + \sigma)}{\sigma(1 - \zeta)} \right), \quad (2.8)$$

the Hopf and pitchfork bifurcations coincide, and the problem has a pair of zero eigenvalues. This point C is a codimension-two Takens–Bogdanov (Takens 1974; Arnol’d 1977; Guckenheimer & Holmes 1983) or ζ^2 (Arnéodo *et al* 1985b) bifurcation point with reflection symmetry. Near this point, the PDEs can be reduced to

the second-order normal form (Knobloch & Proctor 1981; Couillet & Spiegel 1983; Rucklidge 1992):

$$\ddot{v} = \kappa\dot{v} - \lambda v \pm v^3 \pm v^2\dot{v}, \quad (2.9)$$

where v represents the amplitude of convection, and κ and λ are linear combinations of $r - r_C$ and $q - q_C$. The invariance of the normal form under changes of sign of v is a consequence of the reflection symmetry of the original problem. The signs of the cubic coefficients depend on the parameters of the problem.

By considering the limit of narrow rolls (Hughes & Proctor 1990), additional zero eigenvalues are introduced, and the dimension of the centre manifold increases, implying an increase in the order of the normal form describing the problem. Rucklidge (1992) derived a low-order ODE model of magnetoconvection using as an intermediate stage the fifth-order truncation of the PDEs due to Knobloch *et al* (1981), obtaining ODEs that describe the system in this limit:

$$\ddot{v} = \kappa\dot{v} - \lambda v - vw + \mathcal{O}(L^2), \quad \dot{w} = -w + v^2 + \mathcal{O}(L^2), \quad (2.10)$$

where w represents the horizontally averaged temperature. The same ODEs can be obtained using standard perturbation techniques (following Proctor & Weiss 1990), using the width of the rolls as the small parameter. The details of the derivation are given in the Appendix, but essentially, in the limit of arbitrarily narrow rolls, arbitrarily accurate solutions of the PDEs can be constructed from the solutions of the ODE model. The important consequence is that all the bifurcation structure observed in the ODEs (2.10) must be reproduced by the PDEs; in particular, homoclinic bifurcations leading to chaos in the ODEs must also exist and lead to chaos in the PDEs. Using the perturbation method, it is possible to proceed beyond leading order, to obtain corrected model ODEs:

$$\begin{aligned} \ddot{v} &= \kappa\dot{v} - \lambda v - vw + L^2(M_1\dot{v}w + M_2vw + M_3v^3) + \mathcal{O}(L^4), \\ \dot{w} &= -w + v^2 - L^2(v^2 + 4v\dot{v}) + \mathcal{O}(L^4), \end{aligned} \quad (2.11)$$

where M_1 , M_2 and M_3 are constants (given in the Appendix) that depend on σ , ζ and κ . Expressions relating (κ, λ) to (R, Q) are also given in the Appendix. The leading order model (2.10) gives accurate predictions of the behaviour of the PDEs in the limit of narrow rolls, but the prediction of behaviour at small but finite roll width is markedly improved by including the $\mathcal{O}(L^2)$ corrections in (2.11). In addition, the corrected ODEs (2.11) are required when discussing the larger-amplitude behaviour of the PDEs.

The same approach was used by Proctor & Weiss (1990) and by Knobloch *et al* (1992) to derive a third-order model of thermosolutal convection in the limit of narrow rolls; at leading order, their model differs from the one considered here only in the sign of the nonlinearity in the \ddot{v} equation, leading to completely different behaviour from that discussed in this paper.

3. Dynamics of the model ODEs

The uncorrected model ODEs (2.10), introduced by Shimizu & Morioka (1980) as an *ad hoc* model of the Lorenz equations in a regime where $|\lambda| \gg 1$, have been analysed

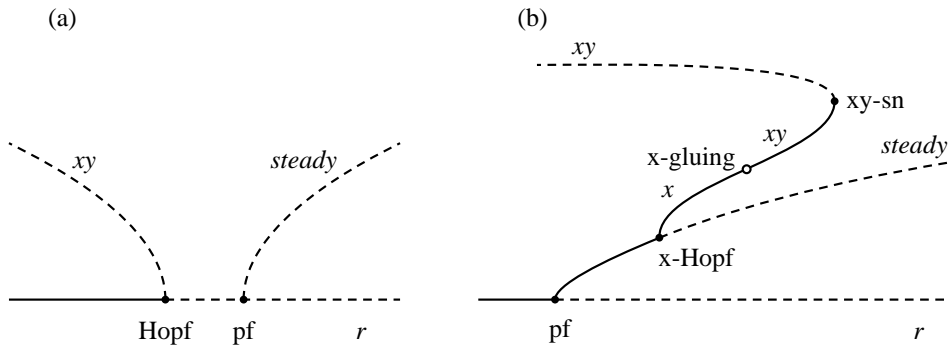


Figure 1. Schematic bifurcation diagrams for the Takens–Bogdanov normal form (2.9) and for the model ODEs (2.10), for two values of q and increasing r : (a) $q > q_C$; (b) $q < q_C$, corresponding to the two dotted lines in Figure 2. The Rayleigh number r is on the horizontal axis and the amplitude of the solution is on the vertical axis. Solid lines represent stable solutions; dashed lines represent unstable solutions. Filled circles represent local bifurcations and open circles represent global (homoclinic or gluing) bifurcations.

by Rucklidge (1993) and Shil’nikov (1986, 1989, 1993); the analysis is briefly recalled here. The ODEs have three equilibrium points: the trivial solution $(v, w) = (0, 0)$, and a symmetric pair of equilibrium points $(v, w) = (\pm\sqrt{-\lambda}, -\lambda)$, which exist only for $\lambda \leq 0$. These two non-trivial solutions correspond to steady convection in the original problem and are related by the reflection symmetry. The bifurcations from the trivial solution are a supercritical pitchfork bifurcation at $\lambda = 0$ and a subcritical Hopf bifurcation at $\kappa = 0$ with $\lambda \geq 0$.

Periodic orbits will be described by symbol sequences of x’s and y’s, indicating how the orbit loops around the right ($v > 0$) or the left ($v < 0$) equilibrium points, following the notation that Sparrow (1982) used for the Lorenz equations. The simplest orbits are the x- and y-orbits, created in a Hopf bifurcation from the nontrivial equilibrium points. These two orbits, which are related by the symmetry of the model, are jointly referred to as the x-orbits. Asymmetric orbits will be prefixed with an A unless there is an odd number of symbols in the sequence (in which case the orbit is bound to be asymmetric). Bifurcations will be prefixed with the simplest orbit involved in the bifurcation; for example, the Hopf bifurcation from the nontrivial equilibrium points, at which the x-orbits are created, is the x-Hopf bifurcation. Similarly, the kneading invariant is defined by computing the one-dimensional unstable manifold of the trivial solution and recording an x (y) for each maximum of w with $v > 0$ ($v < 0$). The kneading invariant changes at homoclinic bifurcations: for instance, in the x-homoclinic bifurcation, the first two symbols of the kneading invariant change from xx to xy. Unfortunately, as in the case of the Lorenz equations, this naming scheme is not a proper global description of trajectories in that it is possible for the description of a periodic orbit to change even though there has been no bifurcation; however, the scheme is useful and will suffice for the purposes of this paper.

If κ and λ are assumed to be small (order ϵ), (2.10) can be reduced to (2.9), the normal form of the Takens–Bogdanov bifurcation with reflection symmetry, by scaling $(v, w, t, \kappa, \lambda) \rightarrow (\epsilon v, \epsilon^2 w, t/\epsilon, \epsilon \kappa, \epsilon^2 \lambda)$ and rewriting the \dot{w} equation as $w = v^2 - \epsilon \dot{w} = v^2 - 2\epsilon v \dot{v} + \mathcal{O}(\epsilon^2)$. When this is substituted into the \ddot{v} equation, (2.9) is recovered. Two bifurcation diagrams (see Figure 1), taken with q fixed and r increasing, illustrate

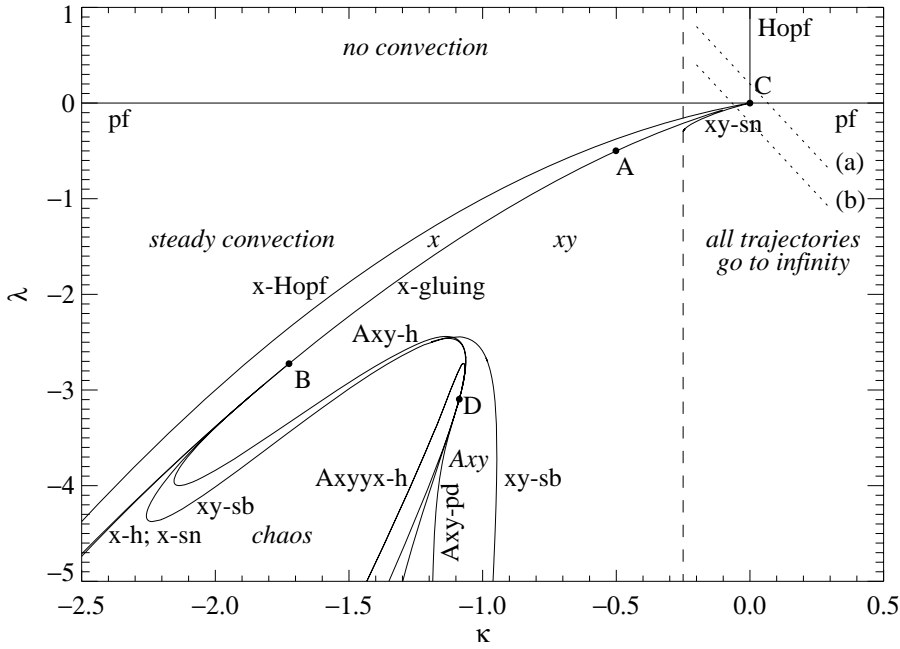


Figure 2. Numerically computed unfolding diagram of (2.10) near the points C and B. The attracting solutions in different regions of the (κ, λ) -plane are indicated in italics; the bifurcation lines are labelled in roman. At B, the x-gluing bifurcation splits into an x-homoclinic bifurcation (x-h), an x-saddle-node (x-sn) bifurcation, an xy-symmetry-breaking (xy-sb) bifurcation and an Axy-homoclinic bifurcation (Axy-h). At D, the Axy-h bifurcation combines with an Axyyx-h bifurcation, producing an Axy-period-doubling (Axy-pd) bifurcation. Schematic bifurcation diagrams taken along the two dotted lines labelled (a) and (b) are shown in Figure 1.

the behaviour of the system in this régime. In Figure 1(a), with $q > q_C$, there is a subcritical Hopf bifurcation; beyond this point, all trajectories escape to infinity. In Figure 1(b), with $q < q_C$, there is a supercritical pitchfork (pf) bifurcation, in which the non-trivial equilibrium points are created. These undergo a supercritical x-Hopf bifurcation, and a pair of x-orbits is created. As r increases further, these asymmetric orbits ‘glue’ together to form a symmetric xy-orbit at a double homoclinic (x-gluing) bifurcation; this new orbit is destroyed at an xy-saddle-node (xy-sn) bifurcation.

The unfolding diagram of (2.10) is presented in Figure 2. Here, κ and λ are more convenient unfolding parameters than r and q ; bifurcation diagrams (for example, Figure 1) taken at constant q correspond to the indicated diagonal slices through the unfolding diagram, sloping downwards to the right. Near the Takens–Bogdanov point C, there are two bifurcations from the trivial solution: the Hopf bifurcation and the pitchfork (pf) bifurcation. The three bifurcation lines emerging from the point C towards negative κ and λ are (from top to bottom), the x-Hopf, the x-gluing and the xy-saddle-node (xy-sn) bifurcations. The xy-saddle-node bifurcation line stops when it reaches the vertical dashed line, along which trajectories of the ODEs become unbounded; this is discussed in more detail in section 5.

The nature of the homoclinic bifurcation depends on the dominant eigenvalues (those eigenvalues, positive or negative, that are closest to zero) of the trivial solution and on the geometry of the homoclinic trajectories. Near the point C in the (κ, λ) plane, the orbits involved in the x-gluing bifurcation are in the figure-of-eight configuration: the homoclinic trajectories approach and leave the trivial solution in the (v, \dot{v}) plane. As the homoclinic bifurcation is followed away from the point C, the two negative eigenvalues of the trivial solution change order (at the point A in Figure 2) and the homoclinic trajectories switch to the butterfly configuration: they approach the trivial solution downwards along the w -axis and leave it in the (v, \dot{v}) -plane. Next, at the point B, the positive eigenvalue in the (v, \dot{v}) plane becomes larger in magnitude than the negative eigenvalue corresponding to the w -axis, so that, beyond the point B, orbits approaching the homoclinic bifurcation must be unstable. The homoclinic bifurcation is no longer a gluing bifurcation, but it splits (or ‘explodes’) into many bifurcations; the four principal ones are shown in Figure 2: an x-homoclinic bifurcation (x-h), an x-saddle-node (x-sn) bifurcation, a subcritical xy-symmetry-breaking (xy-sb) bifurcation and an Axy-homoclinic bifurcation (Axy-h). Chaotic trajectories are found between the two homoclinic bifurcations; this wedge is narrow at first, but broadens as λ decreases. The xy-symmetry-breaking bifurcation becomes supercritical (forming stable Axy-orbits), and the Axy-homoclinic bifurcation is involved in another codimension-two global bifurcation at the point labelled D, which involves more complicated homoclinic bifurcations and the creation of the first of a cascade of period-doubling (pd) bifurcations. For more details, see Rucklidge (1993) and Shil’nikov (1993).

The transition at the point B for symmetric systems in the butterfly configuration such as the PDEs (2.1)–(2.4) or ODEs (2.10) is well understood (Lyubimov & Zaks 1983; Glendinning 1985, 1988; Shil’nikov 1986; Rucklidge 1993). Near this point, the flow can be reduced to a one-dimensional Poincaré map:

$$f : x \rightarrow \text{sign}(x) \left(-\mu + a |x|^\delta \right). \quad (3.1)$$

where x is the coordinate along the unstable eigenvector of the trivial solution, δ is the ratio of the dominant negative eigenvalue to the dominant positive eigenvalue ($\delta = 1$ at B), $-\mu$ is the x -coordinate of the intersection of the unstable manifold of the origin with the Poincaré plane ($\mu = 0$ at the homoclinic bifurcation), and a is a parameter that depends on the global properties of the flow. In the region of interest in (2.10), $\delta = 2/(\kappa + \sqrt{\kappa^2 - 4\lambda})$ and $0 < a < 1$. With $\delta \approx 1$ and x and μ small (that is, near enough to the point B), there is a correspondence between periodic orbits of the map and the flow, and bifurcations in the map correspond to bifurcations in the ODEs. The correspondence is made using symbol sequences, where the symbol x is used when $x > 0$ and y for $x < 0$ in the map.

The map (3.1) is constructed by considering points at which a trajectory of the ODEs successively intersects a Poincaré plane $w = \text{constant}$, so that the flow defines a two-dimensional map from that plane back to itself. The coordinates on the plane are x and y , along and transverse to the unstable direction. The usual approach is to assume that since the transverse direction is strongly contracting, y quickly becomes small and the x coordinate decouples, resulting in (3.1). The reduction can be made rigorous if there is a strong stable foliation, which essentially provides a new set of coordinates (\hat{x}, \hat{y}) of the Poincaré plane that has the property that lines of constant \hat{x} are mapped to each other under iterations of the two-dimensional map. In these

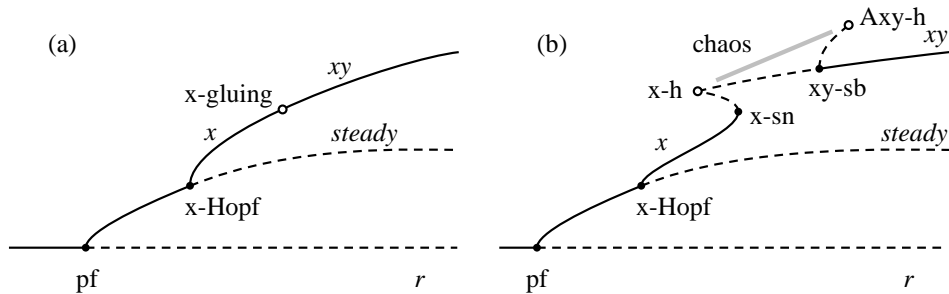


Figure 3. Schematic bifurcation diagrams just (a) above ($\delta > 1$) and (b) below ($\delta < 1$) the point B, showing how the x-gluing bifurcation splits into a pair of homoclinic bifurcations (x-h and Axy-h), with an interval of stable chaos in between.

circumstances, the \hat{y} coordinate decouples exactly, and \hat{x} is governed by a map close to (3.1). While generically there is a stable foliation when $\delta > 1$ and μ is small (Gambaudo *et al* 1992), and if there is one for $\delta < 1$ it is persistent (Robinson 1981), unfortunately there is no guarantee of a stable foliation when δ is near one. However, Robinson (1989, 1992) has shown that there are examples of flows similar to (2.10) and (2.11) that do possess a strong stable foliation near $\delta = 1$. Numerical simulations of the ODEs (2.10) (Rucklidge 1993) and of the PDEs (section 6) suggest that the map (3.1) is an excellent model of the behaviour near the point B.

An analysis of the map leads to the bifurcation diagram in Figure 3: the x-gluing bifurcation in Figure 3(a) splits into an infinite number of homoclinic bifurcations, only two of which are indicated in Figure 3(b). The stable x-orbit turns around in an x-saddle-node (x-sn) bifurcation and is destroyed in the x-homoclinic bifurcation (x-h). The xy-orbit, created in the same homoclinic bifurcation, gains stability in the xy-symmetry breaking (xy-sb) bifurcation; the unstable Axy-orbits created there are destroyed in the Axy-homoclinic (Axy-h) bifurcation. In between the two homoclinic bifurcations there is a parameter interval in which there are attracting chaotic trajectories (a Lorenz attractor). At the point D in Figure 2, the map parameter a passes through zero, and a similar analysis is possible. This point is associated with the conversion of the Lorenz attractor into a quasi-attractor (Shil'nikov 1993).

4. Numerical solution of the PDEs

The PDEs (2.1)–(2.4) were solved numerically using the spectral method with harmonic basis functions. This method was chosen for two reasons: first, because the mildly nonlinear solutions of interest here are approximated well by the linear eigenfunction, and second, because of the similarity between the spectral method and the approach used in constructing the model ODEs.

For this application, the spectral method consists of expanding the fluid variables ω , Ψ , θ and A using the harmonic functions that satisfy the boundary conditions:

$$\Psi(x, z, t) = \sum_{i=1}^n \sum_{j=1}^n \Psi_{ij}(t) \sin k_i x \sin k_j z, \quad (4.1)$$

with similar expressions for ω , θ and A , except that the x basis functions for θ and the z basis functions for A are cosines and the corresponding sums start from zero. The amplitudes Ψ_{ij} , etc. are functions only of time. The wavenumbers are given by $k_i = \pi i/L$ and $k_j = \pi j$. For the range of parameter values of interest in this paper, the amplitudes of all modes with $i + j$ equal to an odd integer decay to zero, so these modes were dropped from the sum (4.1). Retaining only those terms with $i + j \leq n$ (following Veronis 1966) results in a more accurate solution. The spectral expansions were substituted into the PDEs (2.1)–(2.4), and the ODE for each mode amplitude was determined, resulting in a set of equations of the form $\dot{\mathbf{x}} = \mathbf{f}(\mathbf{x})$, where the mode amplitudes make up the elements of the vector \mathbf{x} . The linear terms and derivatives are easy to calculate in spectral space. The nonlinear terms were calculated either spectrally, by an analytic convolution in spectral space, or pseudo-spectrally, by fast Fourier transforms and multiplication in physical space. The two methods agree to within machine accuracy, but the second approach is the more efficient for larger n , especially on vector computers. At least $3n/2$ modes were used in the Fourier transforms, which is sufficient for complete dealiasing, as the nonlinearities are quadratic.

The relative truncation error (RTE) is defined to be the maximum of the ratio of the amplitude of the modes with $i + j = n$ to the amplitude of the primary (1,1) mode, and is a measure of the importance of the modes that have been discarded. This quantity was monitored to ensure accurate numerical solutions; it was found that $n = 12$ was sufficient for the mildly-supercritical calculations reported here. Thus in effect the PDEs are approximated by a high-order set of ODEs: with $n = 12$, there are 120 independent mode amplitudes.

The ODEs for the mode amplitudes are stiff in the limit of narrow rolls (the modulus of the largest negative eigenvalue is $\mathcal{O}(n^2/\varpi)$), so the equations were solved using a semi-implicit extrapolation integrator known as ‘Metan1’ (Bader & Deuffhard 1983). This integrator breaks each timestep down into a progressively larger number of substeps and extrapolates to zero stepsize, until the local relative truncation error estimate is less than a specified tolerance: 10^{-10} was used throughout. Steady solutions were computed using the Newton–Raphson method (Press *et al* 1986) to solve $\mathbf{f}(\mathbf{x}) = \mathbf{0}$, and their stability was determined by computing the eigenvalues of the Jacobian matrix. In this way, steady-state bifurcations could be followed as the parameters were varied. The kneading invariant was computed by taking as the initial condition a small step along the unstable eigenvector of the trivial solution and recording the sign of v at the maxima of w , where v and w were computed from the PDE variables Ψ_{11} and θ_{02} using the expressions in the Appendix. For the parameter range of interest in this paper, homoclinic bifurcations occur where the kneading invariant changes, and could be followed as the parameters were varied.

5. Dynamics of the PDEs: near the point C

In the Takens–Bogdanov normal form (2.9) and the uncorrected model (2.10), the large-amplitude behaviour is unbounded for (κ, λ) near zero, and the unstable branch of xy-orbits in Figure 1(a) and (b) tends to infinity as κ tends to -0.25 from above. Including the $\mathcal{O}(L^2)$ correction terms in (2.11) results in the unstable branch turning around in an xy-saddle-node bifurcation, creating a large-amplitude stable periodic orbit. Table 1 shows how the agreement between the corrected model ODEs and the

Table 1. The xy-orbit at the point C in the corrected model ODEs (2.11) and in the PDEs. For each value ϖ , the maximum of v for the ODEs and for the PDEs is given, along with their ratio and the maximum RTE around the periodic orbit. These data were calculated with $\sigma = 1$, $\zeta = 0.8$. The PDEs were integrated with $n = 12$ modes in each direction – repeating the calculation with $n = 8$ modes yields the same results to three figures, with an RTE about 10^4 times higher.

ϖ	L	v (ODEs)	v (PDEs)	ratio	Max RTE
0.2500	0.2582	1.170	1.000	1.1700	$4.1 \cdot 10^{-10}$
0.1000	0.1601	2.154	2.061	1.0451	$8.6 \cdot 10^{-11}$
0.0500	0.1125	3.195	3.133	1.0198	$1.2 \cdot 10^{-11}$
0.0100	0.0501	7.415	7.389	1.0035	$1.5 \cdot 10^{-14}$
0.0010	0.0158	23.643	23.628	1.0006	$1.2 \cdot 10^{-18}$

PDEs improves as the width of the rolls is decreased: the ratio between the maxima of v around the orbit goes to one as $\varpi \rightarrow 0$. A similar agreement is found between the maxima of w around the orbit. It is interesting to note that v is $\mathcal{O}(L^{-1})$, which implies that the amplitude of the oscillation of the vertical component of the fluid velocity goes to a constant as the width of the rolls goes to zero. The stability of these oscillatory ‘elevator modes’ to disturbances that break the imposed reflecting side boundary conditions has not been investigated, although Proctor & Hughes (1991) have shown that steady narrow rolls can develop a horizontal shearing instability.

The unfolding diagrams of (2.10) and of (2.11) for $\varpi = 0.01$ are shown in Figure 4. The saddle-node and gluing bifurcations in the ODE models were computed using AUTO (Doedel & Kernévez 1986); in the latter case, the homoclinic bifurcation was followed by continuing orbits of very high period. The lines of x-Hopf and x-gluing bifurcations (here computed by approximating the unstable manifold of the origin) were also calculated for the PDEs with $\varpi = 0.01$; these lines are indistinguishable from the results for the corrected ODEs. Figure 5 shows three bifurcation diagrams taken along the three dotted lines marked in Figure 4(b). In Figure 5(a) (with $q > q_C$), the xy-orbits created in the subcritical xy-Hopf bifurcation from the trivial solution gain stability in an xy-saddle-node bifurcation – stable xy-orbits are found to the right of this bifurcation line, labelled xy-sn in Figure 4. As q decreases through q_C (Figure 5b), the xy-Hopf bifurcation climbs onto the branch of steady solutions as before, but now the unstable branch of xy-orbits regains stability in a second xy-saddle-node bifurcation. In Figure 5(c), for even smaller q , these two xy-saddle-node bifurcations have coalesced in a cusp.

The primary Hopf bifurcation to xy-orbits is subcritical just above the Takens–Bogdanov point, but becomes supercritical (in the corrected ODEs) for $\lambda \sim \mathcal{O}(L^{-2})$. As the width of the rolls increases, the point at which the primary Hopf bifurcation becomes supercritical moves towards the Takens–Bogdanov point, and the parameter range over which there are subcritical xy-orbits diminishes. Even in the uncorrected model (Figure 4a), unstable xy-orbits only exist when $-0.25 < \kappa < 0.0$; the line of xy-saddle-node bifurcations terminates in that case at $(\kappa, \lambda) \approx (-0.25, -0.30)$. In subsequent unfolding diagrams, the small region of subcritical xy-orbits will not be mentioned. The saddle-node bifurcation was not computed in the PDEs.

The values of the two diffusivity ratios σ and ζ were fixed at 1.0 and 0.8 respectively for all the narrow roll calculations (section 6). These values were chosen so as to maximise the range of roll widths over which the bifurcation diagrams in Figure 1 are

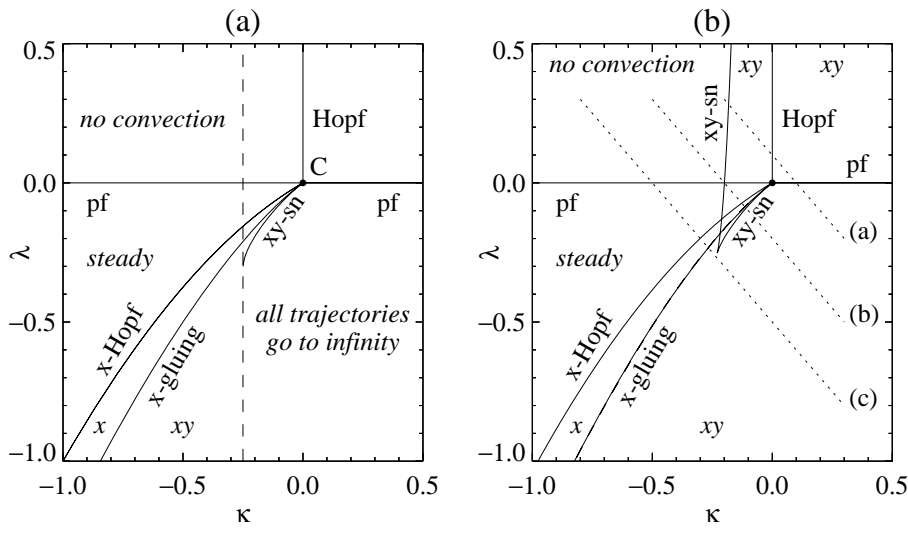


Figure 4. Unfolding diagrams of (a) the uncorrected model ODEs (2.10) and (b) the corrected model ODEs (2.11) with $\varpi = 0.01$, $\sigma = 1.0$ and $\zeta = 0.8$. The attracting solutions in different regions of the (κ, λ) -plane are indicated in italics; the bifurcation lines are labelled in roman. In (a), all trajectories become unbounded as $\kappa \rightarrow -0.25$ (the dashed line). If $\lambda > -0.30$, it is the unstable xy -orbit created in the primary Hopf bifurcation that becomes unbounded, while for $\lambda < -0.30$, it is the stable xy -orbit created in the x -gluing bifurcation that becomes unbounded. In (b), all trajectories remain bounded, and the xy -saddle-node bifurcation line has a cusp. Schematic bifurcation diagrams taken along the three slices in (b), indicated by dotted lines, are shown in Figure 5.

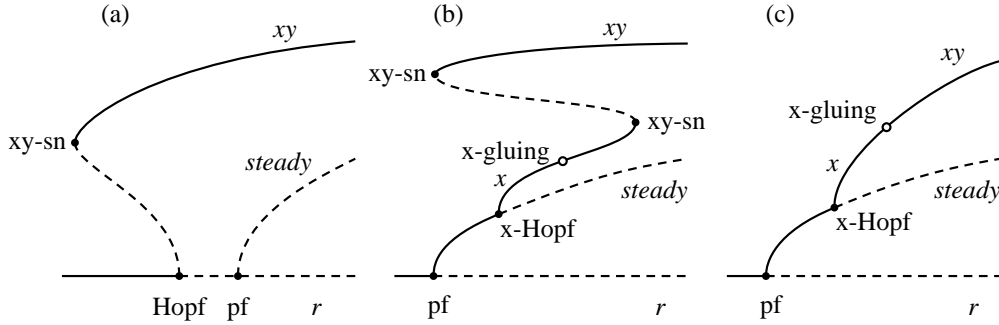


Figure 5. Schematic bifurcation diagrams taken along the three dotted lines marked in Figure 4(b). (a) $q > q_C$; (b) q just below q_C ; (c) beyond the cusp of saddle-node bifurcations.

at least qualitatively correct: with these parameter values and $L \lesssim 0.431$ ($\varpi \lesssim 0.627$), the three bifurcation lines (x -Hopf, x -gluing and xy -saddle-node) emerge from the Takens–Bogdanov point into the third quadrant in the (κ, λ) -plane, and the primary Hopf bifurcation is subcritical. An additional constraint is that the system must not be unstable to rolls narrower than the imposed box width. With these values of σ and ζ , the Takens–Bogdanov point occurs at $(r_C, q_C) = (9, 8)$. The behaviour of the

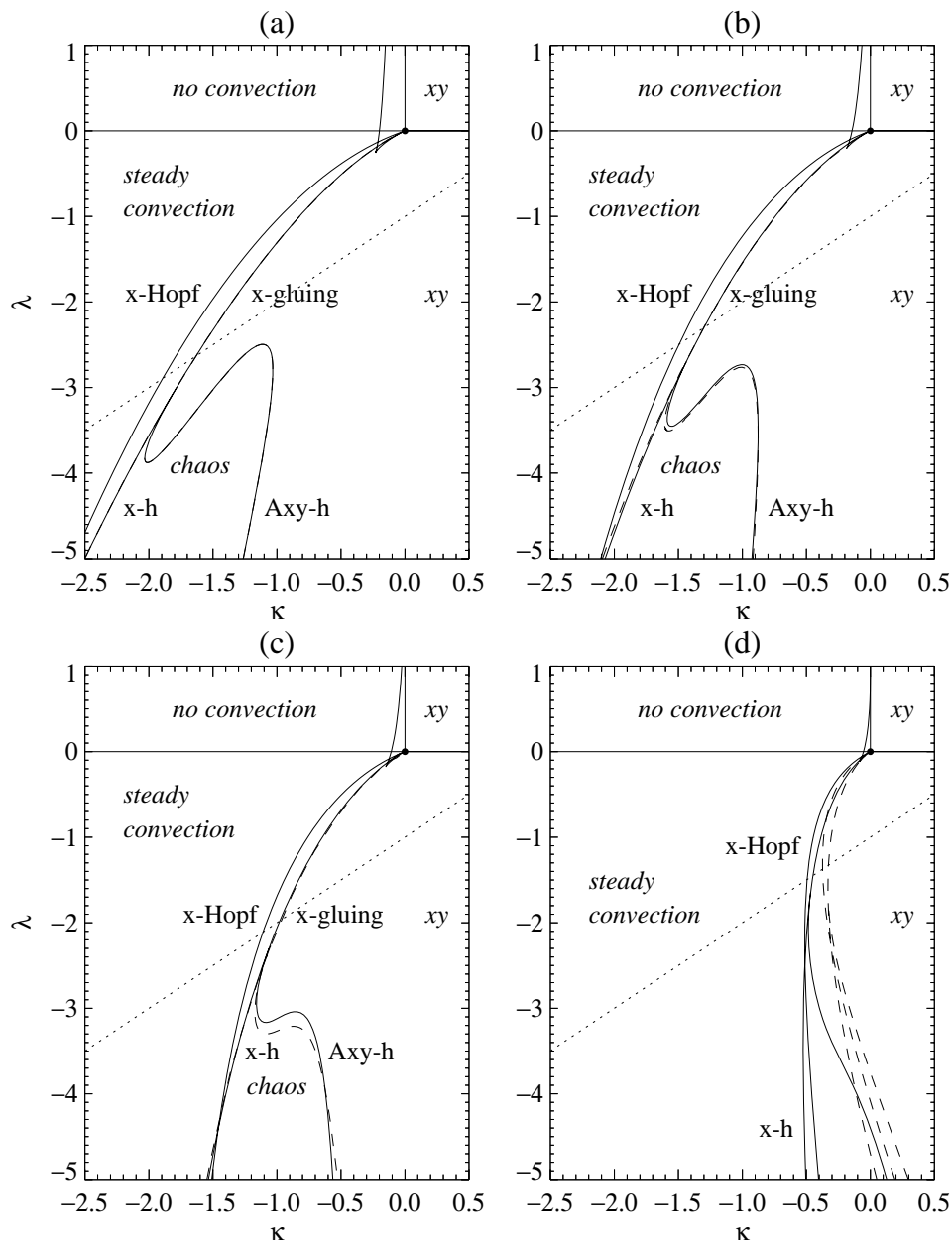


Figure 6. Unfolding diagrams of the corrected model ODEs (2.11) (solid lines) and the PDEs (dashed lines), with $\sigma = 1.0$ and $\zeta = 0.8$. (a) $\varpi = 0.01$; (b) $\varpi = 0.05$; (c) $\varpi = 0.10$; (d) $\varpi = 0.25$. The dotted line indicates where $\delta = 1$ in the ODEs.

system with wider rolls is discussed in section 7.

6. Dynamics of the PDEs: chaos in narrow rolls

The ODE model (2.10) makes quantitative predictions of the locations of bifurcations in the PDEs. The pitchfork and Hopf bifurcations from the trivial solution are given exactly by the relations between (R, Q) and (κ, λ) . The predictions of the other bifurcations are given by (2.10), but are improved by including the $\mathcal{O}(L^2)$ terms in (2.11). Figure 6 shows the (κ, λ) -unfolding plane of (2.11) for four roll widths: $\varpi = 0.01, 0.05, 0.10$ and 0.25 , using the illustrative parameters $\sigma = 1.0$ and $\zeta = 0.8$. In addition to the x-Hopf, x-homoclinic (or gluing) and xy-saddle-node bifurcations that begin at the Takens–Bogdanov point, the Axy-homoclinic bifurcation line was computed; this line begins where the x-gluing bifurcation crosses the dotted line, where $\delta = 1$. The unfolding diagram of (2.10) (Figure 2) is essentially the same as that for $\varpi = 0.01$, shown in Figure 6(a). The locations of the x-Hopf, x-homoclinic and Axy-homoclinic bifurcations in the PDEs were also computed – these are shown as dashed lines in Figure 6. The lines of higher homoclinic bifurcations proved to be too laborious to compute for more than short sections, though the calculations are in principle possible. The agreement between the ODEs (2.11) and the PDEs is remarkably good: for $\varpi = 0.01$ (Figure 6a), the PDE bifurcations lie on top of the ODE bifurcations, to within the width of the line. For $\varpi = 0.05$ and 0.10 (b–c), the corresponding lines only begin to diverge for $\lambda < -3$, while for $\varpi = 0.25$ (d), there is still qualitative agreement: in the PDEs, the Axy-homoclinic bifurcation begins where the x-gluing bifurcation crosses $\delta = 1$, and in the ODEs and PDEs, the lines of x-Hopf and x-homoclinic bifurcations cross near $\lambda = -2.5$. The region of agreement between the PDEs and the ODEs can be translated from (κ, λ) to (r, q) ; for example, with $\varpi = 0.10$, the region depicted in Figure 6(c) translates (approximately) to $3 < q < 9$ and r less than 4% above its critical value.

The most interesting bifurcation from the point of view of discovering chaotic solutions in the PDEs is the x-homoclinic bifurcation. When this line crosses the line where $\delta = 1$, the conditions necessary for the one-dimensional map (3.1) to be a good model of the flow are fulfilled, provided the crossing occurs with $\kappa < 0$. Just beyond the crossing points, there must be an interval of chaotic trajectories between the x- and Axy-homoclinic bifurcations. This chaotic behaviour is demonstrated in Figure 7 for $\varpi = 0.10$ and q fixed at $q = 6.3$, for two parameter values on either edge of the chaotic interval. These data show convincingly how well the chaotic PDE behaviour is captured by the one-dimensional map (3.1). The behaviour of the PDEs matches Figure 3(b) exactly: for $7.3 < r \leq 7.3764595$, all trajectories tend either to the stable steady solutions or to a stable x-orbit; this is followed by a chaotic interval, then for $r \geq 7.376469$ all trajectories tend to a stable xy-orbit.

Figure 7(a)–(d) are at $r = 7.3764597$, just beyond the x-homoclinic bifurcation, showing the chaotic manner in which the system alternates between clockwise and counter-clockwise (v positive and negative respectively) rolls. Note that the kneading invariant may be read from (b). Even though the trajectory in (a) does not appear to be chaotic, its true nature is revealed in (c), which shows an enlargement near the origin. The value of v is recorded each time the trajectory intersects the plane $w = 0.001$; this value of v is plotted against the subsequent value of v , resulting in a one-dimensional return map from the integration of the PDEs, shown as crosses in Figure 7(d). These data are fitted to the predicted form of the map (3.1) using the value of δ computed from the eigenvalues of the trivial solution of the PDEs, the resulting map being the (scarcely visible) solid line in (d). The fitting was a

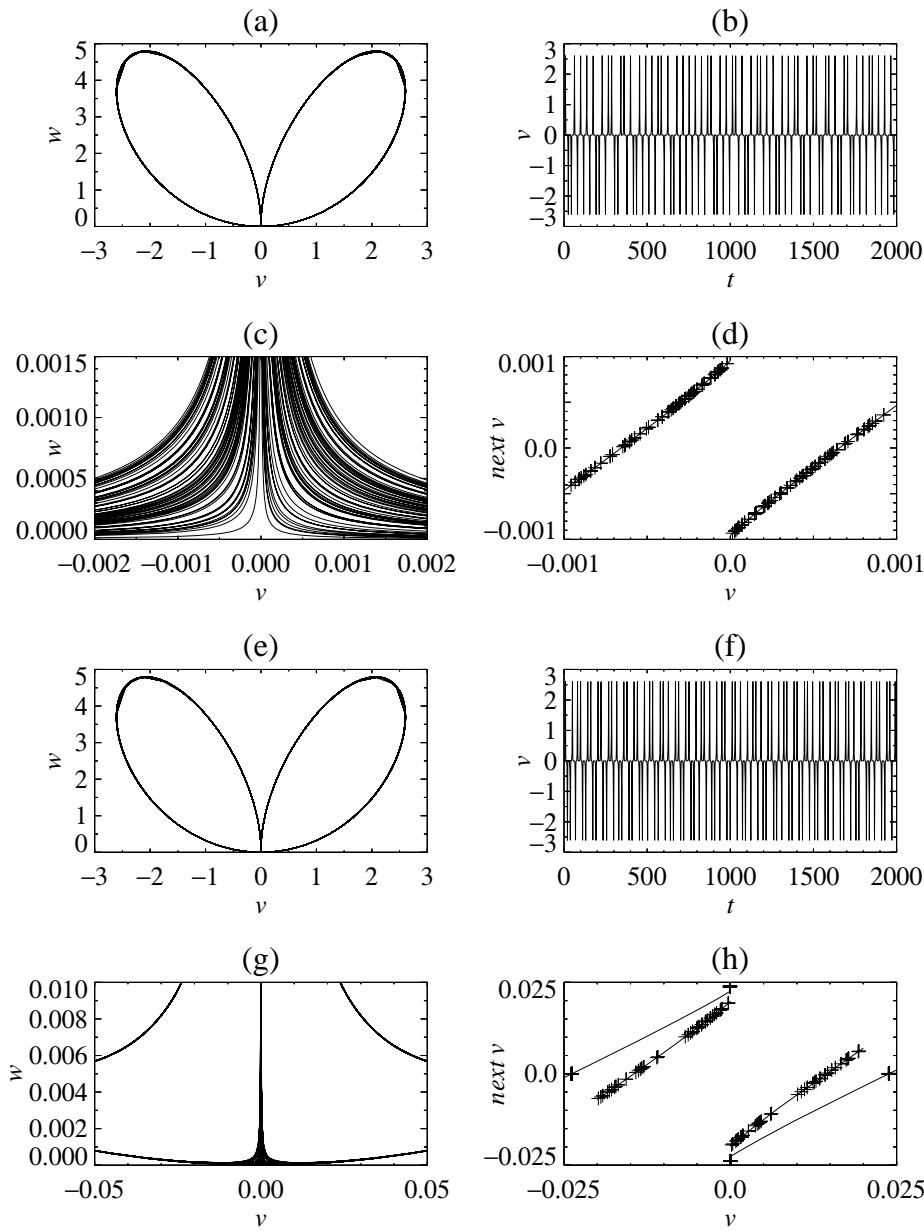


Figure 7. Examples of chaotic trajectories in the PDEs with $\sigma = 1.0$, $\zeta = 0.8$ and $q = 6.3$. (a)–(d) are for $r = 7.3764597$ near the x-homoclinic bifurcation, and (e)–(h) are for $r = 7.376468$ near the Axy-homoclinic bifurcation. (a,e) Phase portraits: w plotted against v . (b,f) Time series: v against time. (c,g) Details of the phase portraits near the origin. (d,h) Return maps: the crosses indicate the values of v at which the trajectory in the PDEs intersects a plane $w = \text{const}$, and the solid line indicates the map (3.1) with fitted map parameters. In (d), $w = 0.001$, $\delta = 0.93764$ and fitted map parameters $\mu = 0.000958$ and $a = 0.925$. In (h), the return plane is $w = 0.010$ and the map parameters are $\delta = 0.93757$, $\mu = 0.0226$, $a = 0.752$; also shown in (h) is the renormalized return map (the inner graph, expanded by a factor of twenty), using a return plane $w = 0.001$, with fitted map parameters $\mu = 0.000990$ and $a = 0.871$.

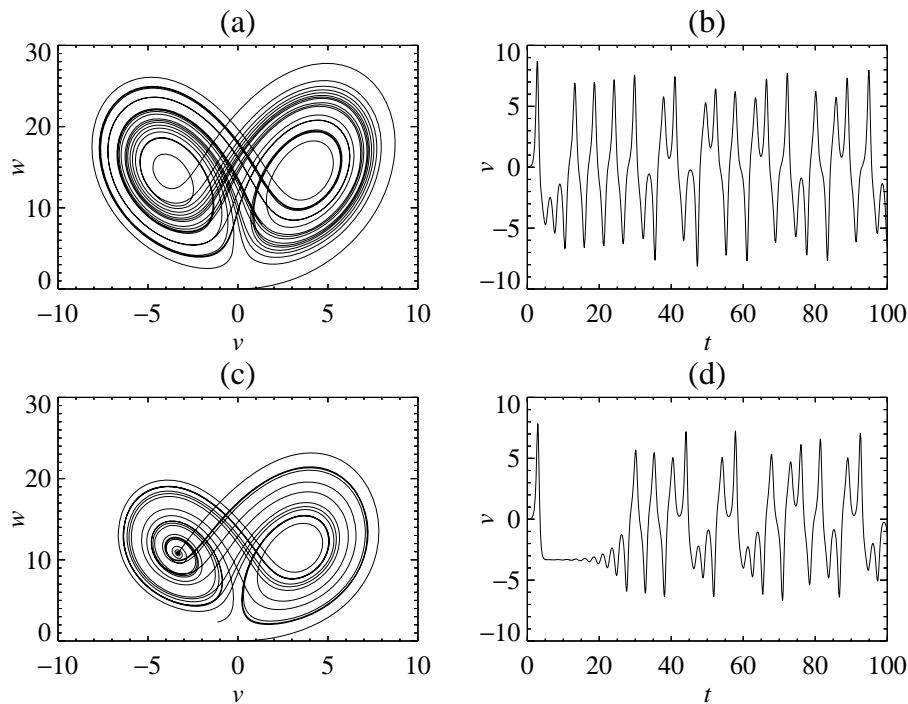


Figure 8. Examples of trajectories of (a)–(b) the PDEs and (c)–(d) the corrected ODEs with $\sigma = 1.0$, $\zeta = 0.8$ and $\varpi = 0.10$, and the parameters (κ, λ) chosen close to the T-point in the ODEs: $(\kappa, \lambda) = (-0.88, -11.0)$. The corresponding PDE parameters are $(r, q) = (6.80847, 5.4373)$. Phase portraits are shown in (a) and (c); time series are shown in (b) and (d).

linear least-squares fit of (3.1), plotting $f(x)$ against $|x|^\delta$. Similarly, Figure 7(e)–(g) are at $r = 7.376468$, just before the Axy-homoclinic bifurcation. The wide lacuna (gap) is evident in the chaotic attractor (Figure 7g), indicating that the dynamics is renormalizable (Glendinning & Sparrow 1993). The map obtained using $w = 0.010$ as the return plane is shown in (h); renormalizing is effected by dropping every other return to this plane, or by using $w = 0.001$, within the lacuna – the resulting renormalized map is also shown in (h), enlarged by a factor of twenty. In fact, the renormalized map also has a narrow lacuna (a gap in the distribution of crosses), indicating that a second renormalization is possible. This implies that the sequence of x’s and y’s in the kneading invariant (see Figure 7f) can be grouped into a chaotic sequence of $xyyx$ ’s and $yxyx$ ’s. For $r \geq 7.376469$, trajectories tend to an xy -orbit.

As r continues to increase, there is a second interval of chaotic solutions that begins with an xy -symmetry-breaking and an Axy-homoclinic bifurcation ($r \approx 7.42$), corresponding to the line $q = 6.3$ entering the upward lobe of the Axy-homoclinic bifurcation in Figure 6(c). As r increases beyond this point, one must be careful about the numerics: the RTE has so far remained below 10^{-9} for the $n = 12$ truncation (recall that r is only 1.6% above its critical value of 7.3), but this second interval of chaotic oscillations persists to $r \approx 12.6$, where the RTE is 0.02. We have not attempted to follow accurately the PDEs in this régime, but merely state that with the truncation fixed at $n = 12$, the steady solution regains stability in a Hopf bifurcation at $r \approx 13.2$.

The model ODEs (2.10) are capable of much more complicated behaviour. At $(\kappa, \lambda) \approx (-2.000000, -6.562500)$, there is a T-point, at which there are heteroclinic connections between all three fixed points, and the two non-trivial fixed points are saddle-foci (Glendinning & Sparrow 1986; Bykov 1978, 1993). In the corrected ODEs (2.11) with $\varpi = 0.10$, the T-point occurs at $(\kappa, \lambda) \approx (-0.8795480, -11.03450)$. Figure 8 shows solutions of the PDEs and of (2.11) at parameter values near the T-point in the ODEs. In the ODEs, one heteroclinic connection is evident as the unstable manifold of the origin comes very close to the unstable nontrivial fixed point; trajectories close to the one computed will return to a neighbourhood of the origin. The PDEs are clearly near, but not at, their T-point, (the unstable manifold of the origin misses the nontrivial fixed point) but this is not surprising considering the magnitude of ϖ . No doubt there is a T-point in the PDEs for nearby parameter values. Similar calculations done with smaller values of ϖ show a much closer agreement, but it is interesting to see the narrow-roll predictions for individual parameter values persisting up to rolls about one sixth as wide as they are high.

The chaotic dynamics observed near $\delta = 1$ (Figure 7) is due to the existence of a Lorenz attractor, which may be modelled reliably by the one-dimensional map (3.1). On the other hand, the chaotic dynamics observed near the T-point (Figure 8) is due to the existence of a quasi-attractor, which cannot in principle be modelled reliably (Gonchenko *et al* 1993). This implies that the details of the dynamics near the T-point will be sensitive to the terms that were discarded from the model, as well as to truncation and numerical errors introduced when solving the PDEs, so it is pointless to continue the comparison between the PDEs and the ODEs any further.

As the x-homoclinic bifurcation is followed further from the origin, it eventually swings into the $\kappa \geq 0$ half-plane (see for example Figure 6d). Moreover, for wider rolls, the point at which the x-gluing bifurcation crosses the line $\delta = 1$ (which corresponds to $\lambda = \kappa - 1$ in the model ODEs) occurs at values of κ closer to zero. Eventually, the x-gluing bifurcation must cross the line $\delta = 1$ exactly at $\kappa = 0$, at which point there is a codimension-three homoclinic bifurcation: all three eigenvalues of the origin are equal in magnitude. This occurs when $\varpi \approx 0.747$ in the corrected ODEs, but for narrower rolls in the PDEs. As long as the rolls are narrower than this, the prediction of the existence of the Lorenz attractor in the PDEs remains good. In wider rolls, when the line of x-gluing bifurcations crosses into the $\kappa \geq 0$ half-plane before crossing the line $\delta = 1$, the gluing bifurcation must occur on an unstable portion of the branch of x- and xy-orbits, since when $\kappa > 0$, the unstable eigenvalue of the origin is greater in magnitude than the stable eigenvalues. There is thus a codimension-two gluing bifurcation (of the type analysed by Rodríguez-Luis *et al* 1991), at which a pair of saddle-node bifurcations are created in essentially the same way as discussed by Rucklidge *et al* (1993). Unlike in the case of narrower rolls discussed above, this unstable gluing bifurcation does not involve chaotic trajectories since the orbits are in the figure-of-eight (not the butterfly) configuration, and the dynamics near the gluing bifurcation is essentially two-dimensional. The codimension-three homoclinic bifurcation could be analysed in terms of the map of Lyubimov & Byelousova (1993), but this is beyond the scope of this paper.

7. Dynamics of the PDEs: wider rolls

The ODEs (2.10) used in the previous sections to model the behaviour of the PDEs in the limit of narrow rolls fail as the roll width becomes larger. When the rolls are

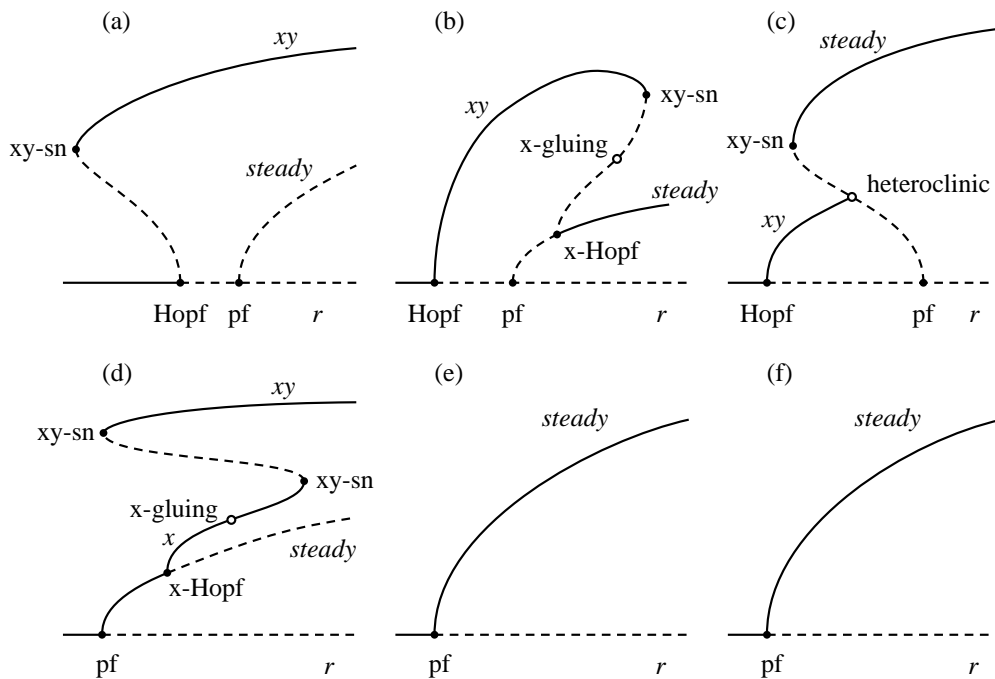


Figure 9. Schematic bifurcation diagrams of (7.1) with q fixed above (a–c) and below (d–f) q_C . (a,d) Narrow rolls: $M > 0$ and $N < 0$. (b,e) Medium rolls: $M > 0$ and $N > 0$. (c,f) Wide rolls: $M < 0$ and $N > 0$.

wider than $L = 0.431$ ($\varpi = 0.627$) using the illustrative parameter values $\sigma = 1.0$ and $\zeta = 0.8$, even the qualitative description of the behaviour of the PDEs near the Takens–Bogdanov point (Figure 1) is incorrect. The reason for this failure is that the coefficients of the cubic terms in the Takens–Bogdanov normal form (2.9) change sign as the width of the rolls increases.

The behaviour of the PDEs as the cubic coefficients change sign is captured by the model of Rucklidge *et al* (1993), who considered compressible convection in a vertical magnetic field, with similar values of all the physical parameters. They modified (2.9) to include appropriate quintic terms:

$$\ddot{v} = \kappa \dot{v} - \lambda v + M v^3 + N v^2 \dot{v} - v^5 - v^4 \dot{v}. \quad (7.1)$$

The quintic terms are those that would appear in a problem with reflection symmetry if the coefficients of the cubic terms (M and N) were zero. The signs of the quintic terms were chosen to prevent trajectories going to infinity regardless of the values of M and N . The signs of M and N give the behaviour at the primary pitchfork and Hopf bifurcations respectively: if the coefficient is positive, the corresponding bifurcation is supercritical. The cubic coefficients were calculated by Knobloch & Proctor (1981): M is negative and N is positive in the limit of narrow rolls, and as the roll width increases, first N changes sign (at $L = 0.431$ when $\sigma = 1.0$ and $\zeta = 0.8$), then M changes sign (at $L > 1.0$ regardless of the values of σ and ζ). In the model (2.11), N changes sign at $L = 0.665$ ($\varpi = 1.23$), and M does not change sign.

The behaviour of (7.1) in the three parameter régimes is given in Figure 9: the behaviour in the limit of narrow rolls (a and d) has been discussed in section 5

(Figure 5). In medium-width rolls with $q > q_C$ (Figure 9b), the xy-orbit is created in a supercritical Hopf bifurcation and rejoins the steady branch in a saddle-node, ungluing and subcritical Hopf bifurcation sequence. Rucklidge *et al* (1993) suggest that the xy-orbit in the narrow-roll case (Figure 9a,d) will rejoin the steady branch in the same manner in the medium roll case (Figure 9b). With $q < q_C$ in the medium and wide cases (Figure 9e,f), there is only the primary pitchfork bifurcation, though there may subsequently be a bubble of unsteady behaviour. Finally, in the case of wide rolls with $q > q_C$ (Figure 9c), the xy-orbit is destroyed in an xy-heteroclinic bifurcation when it collides with the branch of unstable steady solutions, which gains stability in a saddle-node bifurcation. The transition between the medium and wide roll cases is discussed by Dangelmayr *et al* (1985), who included only the v^5 term in (7.1). Here, the $v^4\dot{v}$ term is required to allow the subcritical oscillatory branch to gain stability in a saddle-node bifurcation, and so model the narrow-medium transition.

Weiss (1981) solved the PDEs numerically for a variety of parameter values near the Takens–Bogdanov point, and found behaviour consistent with Figure 9(b) and (c), familiar from the work of Knobloch *et al* (1981), who studied a fifth-order truncation of the PDEs for convection in a vertical magnetic field. The bifurcation structure of that truncation has been explored by Knobloch & Weiss (1983), who reported the development of chaotic solutions associated with a heteroclinic connection between a pair of saddle-foci (the unstable steady solutions) with a real positive eigenvalue larger in magnitude than the real part of a pair of stable complex eigenvalues.

The starting point of a search for chaotic oscillations in the PDEs must be in parameter régimes where it can be established that there are global connections, that is, at the Takens–Bogdanov point. In the earlier part of this paper, the gluing bifurcation in Figure 9(d) was successfully followed into a parameter régime where the eigenvalues were ordered in the manner necessary for chaotic oscillations. In the case of rolls of medium width, the global bifurcation occurs on the unstable branch, so any associated chaotic oscillations will not be attracting. The wide roll case offers more hope: up to the heteroclinic bifurcation in Figure 9(c), the xy-orbit is attracting, so any chaotic trajectories associated with this global bifurcation ought to be attracting for at least some parameter values. Beyond the global bifurcation, all trajectories are attracted to the large-amplitude steady solution.

As yet, the only suggestion that the chaos that Knobloch & Weiss (1983) found in the fifth-order truncated model may also be found in the PDEs was made by Weiss (1981), who found, at one set of parameter values, aperiodic behaviour that did not settle down to regular oscillations after ten cycles. We have repeated Weiss’s calculations, and find chaotic trajectories at and near his parameter values. In the remainder of this section, Weiss’s parameter values are used: $\sigma = 1.0$, $\zeta = 0.1$ and $\varpi = 2.0$ ($L = 1$). For these values, the cubic coefficients in (7.1) satisfy $M > 0$ and $N < 0$ so near the Takens–Bogdanov point, the appropriate bifurcation diagrams are Figure 9(b) and (e). However, numerical experiments on the truncated model suggest that it is only for values of q extremely close to (and just above) the codimension-two value q_C that the system behaves as in Figure 9(b) – the steady branch almost immediately goes through a saddle-node bifurcation and descends to smaller r before regaining stability in a second saddle-node bifurcation. Additionally, the xy-orbit created in the primary Hopf bifurcation is destroyed in a heteroclinic bifurcation when it collides with the unstable steady branch (Knobloch *et al* 1992). Therefore, the most useful bifurcation diagram to consider is Figure 9(c), which describes the essentials of the behaviour of the truncated model for $q \gtrsim q_C$ (with the addition of a minor

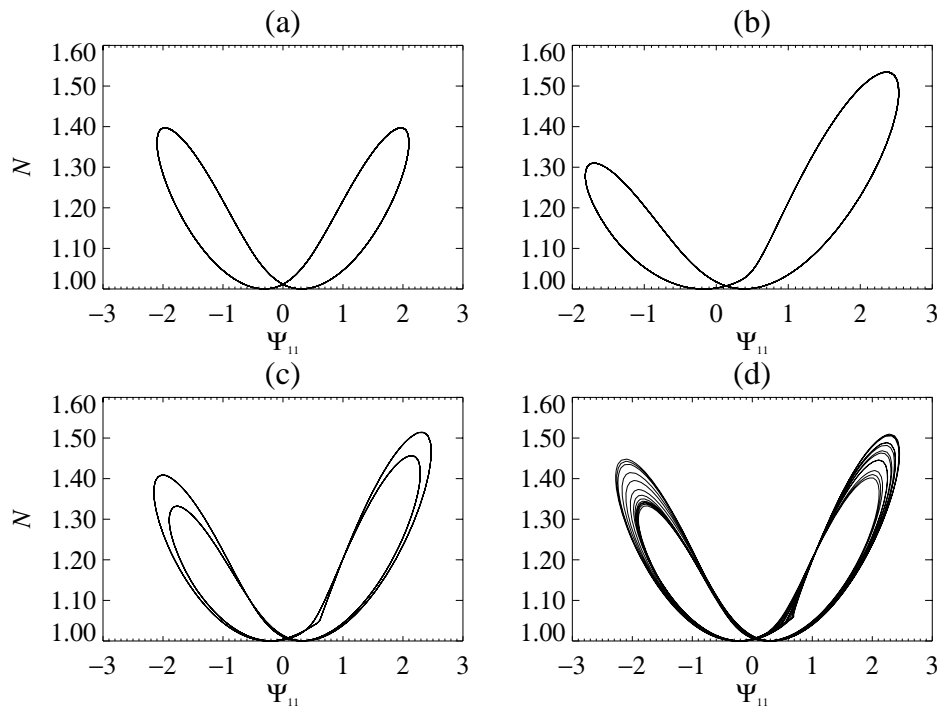


Figure 10. Solutions of the PDEs with $\sigma = 1.0$, $\zeta = 0.1$, $\varpi = 2.0$ and $q = 2.5$: (a) $r = 2.30$; (b) $r = 2.38$; (c) $r = 2.41$; (d) $r = 2.42$, showing the development of chaos through a symmetry-breaking/period-doubling sequence.

supercritical detour of the steady branch).

We investigate the possible chaotic behaviour of the PDEs with rolls of square cross-section by beginning with the global bifurcation that emerges from the Takens–Bogdanov point at $(r_C, q_C) = (1.22, 0.22)$. We do not attempt a complete study of this problem, but only calculate three slices through the (r, q) -plane, following the periodic orbit created in the Hopf bifurcation until it is destroyed in a heteroclinic bifurcation with the unstable steady solutions. A fixed truncation was used for solving the PDEs ($n = 12$), which kept the RTE below 10^{-2} . Some of the calculations were redone with $n = 20$, with no significant change in the observed behaviour and an RTE less than 10^{-4} .

With $q = 1.0$, the Hopf bifurcation occurs at $r = 1.265$; the periodic orbit is destroyed at $r \approx 1.680$ when it collides with the unstable fixed point created in the pitchfork bifurcation at $r = 2.0$ (as in Figure 9c). At the heteroclinic bifurcation, the relevant eigenvalues of the fixed point have ratio $\delta \approx 2.04$, where δ is the absolute ratio of the real part of the dominant negative eigenvalue to the positive eigenvalue. The steady solution persists down to $r \approx 1.636$ before turning around in a saddle-node bifurcation. Further from the Takens–Bogdanov point, with $q = 2.0$, there is a bubble of symmetry-broken oscillations around $r = 2.0$, and the periodic orbit is destroyed in a heteroclinic bifurcation at $r \approx 2.131$, this time with $\delta \approx 1.92$. The steady solution turns around in a saddle-node bifurcation at $r \approx 2.101$. Finally, with $q = 3.0$, the symmetric periodic orbit (Figure 10a) undergoes a symmetry-breaking bifurcation (b),

followed by a period-doubling bifurcation (c) leading to chaotic oscillations (d) at $r = 2.42$. This is followed by an inverse period-doubling cascade, and for $r \gtrsim 2.539$, ($\delta \approx 1.78$), trajectories tend to the large-amplitude steady solution, created in a saddle-node bifurcation at $r \approx 2.512$.

In the chaotic intervals described above, the eigenvalue ratio δ of the unstable steady solution does not satisfy Shil'nikov's (1965) criterion for the existence of chaotic solutions at the heteroclinic bifurcation ($\delta < 1$), even though apparently chaotic trajectories are observed numerically; in fact, chaotic trajectories are observed before the steady solution has even been created in its saddle-node bifurcation (as in, for example, Figure 10d). However, Glendinning & Sparrow (1984) point out that when δ is not much greater than 1, chaotic behaviour is often found, even though the asymptotic behaviour as the heteroclinic bifurcation is approached is not chaotic. The aperiodic solution that Weiss (1981) found was at $r = 2.25$ and $q = 2.53$; our calculations support Weiss's suggestion that the PDEs for convection in a vertical magnetic field have chaotic trajectories, and vindicate prediction of chaotic solutions made by the fifth-order truncated model of Knobloch *et al* (1981).

This route to chaos, associated with a Shil'nikov bifurcation, has been observed in the PDEs for two-dimensional thermosolutal convection (Knobloch *et al* 1986), and investigated in detail in an asymptotically exact model (Proctor & Weiss 1990) and a truncated model (Knobloch *et al* 1992) of the same system. In that case, as in this, there is a codimension-two bifurcation where the eigenvalue ratio satisfies $\delta = 1$ at the heteroclinic bifurcation, when it is followed away from the Takens–Bogdanov point. This codimension-two global bifurcation, with complex eigenvalues, has been studied by Healey *et al* (1991) and by Freire *et al* (1993), but a complete analysis has not yet been carried out.

8. Conclusion

We have studied the transition to chaos in the PDEs (2.1)–(2.4) for two-dimensional Boussinesq magnetoconvection, using a combination of analytical and numerical techniques. In the limit of narrow rolls, the ODE model (2.10) provides an asymptotically exact description of the behaviour of the PDEs near the Takens–Bogdanov point. The transition to chaos occurs in this model at a codimension-two global bifurcation, near which point the dynamics is well described by the one-dimensional Lorenz map (3.1). In this limit, the bifurcations of the PDEs must be the same as those of the ODEs; independently, the arguments that lead to the Lorenz map in the ODEs apply to the situation in the PDEs as well, demonstrating that the PDEs have chaotic trajectories originating in the same codimension-two global bifurcation. Near this bifurcation point, numerically computed solutions of the PDEs are well described by the Lorenz map. This is the first time that the nature of chaotic oscillations observed numerically in PDEs has been established firmly.

The ability of the ODE model (2.10) to describe accurately the behaviour of the PDEs in rolls of finite width is markedly improved by including first-order corrections in (2.11). Calculations of trajectories at the Takens–Bogdanov point in the PDEs and in the corrected model ODEs agree in the limit of narrow rolls, and the corrected ODEs are able to track the locations of the bifurcations in the PDEs over a considerable region of parameter space. The locations of the principal bifurcation lines vary smoothly with the width of the rolls, and the PDEs have a T-point at parameter values

near the T-point in the ODEs. Since the T-point is associated with the transition from a Lorenz attractor to a quasi-attractor in (2.10) (Shil'nikov 1993; Bykov & Shil'nikov 1992), and since Gonchenko *et al* (1993) have proved that the existence of a quasi-attractor in a system implies that the details of the bifurcation sequences will depend sensitively on the parameters in the problem (and on the terms that were discarded in (2.11)), it is pointless to pursue the comparison between the PDEs and the model ODEs any further. The only exception to this would be to work out how the Lorenz attractor vanishes as the width of the rolls increases, but this is not attempted in this paper.

The global bifurcation that leads to chaotic dynamics is on the stable part of the oscillatory branch in the case of narrow rolls. With rolls of medium width, this global bifurcation moves onto the unstable part of the oscillatory branch (Rucklidge *et al* 1993), while in the case of wide rolls, the stable oscillatory branch collides with the unstable steady branch in a heteroclinic bifurcation. In that case, attracting chaotic trajectories arise once the eigenvalues are ordered appropriately, or even before. It may be that this heteroclinic connection between the unstable steady solutions in the wide-roll case is related to the heteroclinic connection between the same unstable steady solutions that is created at the T-point, but more calculations would be required to elucidate this relationship.

In this paper, we have considered the behaviour of the PDEs for two-dimensional Boussinesq convection in the presence of a vertical magnetic field, assuming no instabilities to modes that break the imposed spatial symmetries and two-dimensionality. If the fluid is confined to a box with reflecting side boundary conditions, then the only possible two-dimensional symmetry-breaking instability is to asymmetric rolls, which could be modelled by including terms proportional to $\sin(2\pi x/L) \sin \pi z$ in the stream-function (Nagata *et al* 1990). If periodic side boundary conditions had been used instead, there are two other two-dimensional instabilities: to sheared/tilted rolls, if a term like $\cos(2\pi x/L) \sin \pi z$ is included in the stream-function (Matthews *et al* 1993), and to travelling waves, if a term like $\cos(\pi x/L) \sin \pi z$ is included (Dangelmayr & Knobloch 1986). In the first two of these three instabilities, the linear instability boundary is far away from the Takens–Bogdanov point in the limit of narrow rolls. Rucklidge & Matthews (1993, 1995) have used the same technique of taking the limit of narrow rolls (but with small magnetic field) with periodic boundary conditions, and obtained a fifth-order truncation of magnetoconvection that exhibits a variety of complicated global bifurcations; their model is in qualitative agreement with PDE simulations. The instability to travelling waves has been analysed by Matthews & Rucklidge (1993), who show that near the Takens–Bogdanov point in the limit of narrow rolls, travelling waves are unstable to standing waves. Thus we expect to observe the chaotic trajectories described in this paper even if the imposed spatial symmetries are relaxed.

The three-dimensional instabilities pose a greater problem. Clune & Knobloch (1994) have calculated the preferred form of three-dimensional convection at onset. Steady convection always sets in as rolls, so the instabilities of rolls that lead to chaos are not excluded, but, as the analysis of the Takens–Bogdanov bifurcation in the three-dimensional case has yet to be performed, it may be that three-dimensional instabilities occur before the bifurcations described in this paper.

Acknowledgments

I am most grateful to Nigel Weiss for his guidance and encouragement. I am also grateful for useful suggestions and comments from Paul Glendinning, Keith Julien, Edgar Knobloch, Paul Matthews, Michael Proctor, William Rucklidge, Andrey Shil'nikov and Colin Sparrow. This research was supported by the Science and Engineering Research Council and by Peterhouse, Cambridge.

Appendix. Derivation of the model ODEs

The model ODEs (2.10) may be derived directly from the PDEs for Boussinesq convection in a vertical magnetic field (2.1)–(2.4), using standard perturbation techniques (Malkus & Veronis 1958). The width of the rolls, L , is taken as the small parameter; (R, Q) are required to be near the codimension-two bifurcation point (R_C, Q_C) :

$$R = R_C(1 + L^2 r_2 + L^4 r_4 + L^6 r_6 + \dots), \quad Q = Q_C(1 + L^2 q_2 + L^4 q_4 + L^6 q_6 + \dots), \quad (\text{A.1})$$

where

$$(R_C, Q_C) = \left(\frac{\pi^4(\sigma + \zeta)(1 + L^2)^3}{L^4\sigma(1 - \zeta)}, \frac{\pi^2\zeta(1 + \sigma)(1 + L^2)^2}{L^4\sigma(1 - \zeta)} \right). \quad (\text{A.2})$$

The horizontal coordinate x is scaled to Lx and time t is scaled by a factor of $1/4\pi^2$. An examination of the balance between the terms in the PDEs leads to the expansions:

$$\Psi = L^2(\Psi_0 + L\Psi_1 + L^2\Psi_2 + L^3\Psi_3 + L^4\Psi_4 + L^5\Psi_5 + L^6\Psi_6 + \dots), \quad (\text{A.3})$$

$$\theta = L^3(\theta_0 + L\theta_1 + L^2\theta_2 + L^3\theta_3 + L^4\theta_4 + L^5\theta_5 + L^6\theta_6 + \dots), \quad (\text{A.4})$$

$$A = L^4(A_0 + LA_1 + L^2A_2 + L^3A_3 + L^4A_4 + L^5A_5 + L^6A_6 + \dots), \quad (\text{A.5})$$

where Ψ_0 etc. are functions of x, z and t . Substituting these expansions into the PDEs and equating powers of L results in the leading-order linear equation:

$$\sigma \frac{\partial^4 \Psi_0}{\partial x^4} + \sigma R_0 \frac{\partial \theta_0}{\partial x} + \sigma \zeta Q_0 \frac{\partial^3 A_0}{\partial x^2 \partial z} = 0, \quad (\text{A.6})$$

$$\frac{\partial \Psi_0}{\partial x} + \frac{\partial^2 \theta_0}{\partial x^2} = 0, \quad (\text{A.7})$$

$$\frac{\partial \Psi_0}{\partial z} + \zeta \frac{\partial^2 A_0}{\partial x^2} = 0, \quad (\text{A.8})$$

where (R_0, Q_0) are the leading-order terms in (R_C, Q_C) :

$$(R_0, Q_0) = \left(\frac{\pi^4(\sigma + \zeta)}{L^4\sigma(1 - \zeta)}, \frac{\pi^2\zeta(1 + \sigma)}{L^4\sigma(1 - \zeta)} \right). \quad (\text{A.9})$$

Define \mathcal{L} to be the linear differential operator defined by equations (A.6)–(A.8), which have two independent solutions that satisfy the boundary conditions:

$$\begin{pmatrix} \Psi_0 \\ \theta_0 \\ A_0 \end{pmatrix} = \begin{pmatrix} a_0(t) \sin \pi x \sin \pi z \\ (a_0(t)/\pi) \cos \pi x \sin \pi z \\ (a_0(t)/\zeta\pi) \sin \pi x \cos \pi z \end{pmatrix} \quad \text{and} \quad \begin{pmatrix} \Psi_0 \\ \theta_0 \\ A_0 \end{pmatrix} = \begin{pmatrix} 0 \\ C_0(z, t) \\ 0 \end{pmatrix}, \quad (\text{A.10})$$

where $a_0(t)$ and $C_0(z, t)$ are as yet undetermined functions. The existence of the first solution requires that $R_0 = \pi^2 Q_0 + \pi^4$. The general solution at leading order is then the sum of these two independent solutions. At first order, the equation

$$\mathcal{L} \begin{pmatrix} \Psi_1 \\ \theta_1 \\ A_1 \end{pmatrix} = \mathbf{0} \quad (\text{A.11})$$

has the solution

$$\begin{pmatrix} \Psi_1 \\ \theta_1 \\ A_1 \end{pmatrix} = \begin{pmatrix} a_1(t) \sin \pi x \sin \pi z \\ (a_1(t)/\pi) \cos \pi x \sin \pi z + C_1(z, t) \\ (a_1(t)/\zeta \pi) \sin \pi x \cos \pi z \end{pmatrix}, \quad (\text{A.12})$$

where $a_1(t)$ and $C_1(z, t)$ are as yet undetermined functions. However, a_1 can be included in a_0 , so a_1 is set to 0. At second order, the equation

$$\mathcal{L} \begin{pmatrix} \Psi_2 \\ \theta_2 \\ A_2 \end{pmatrix} = \begin{pmatrix} \pi^4 (((\sigma + \zeta)r_2 - \zeta(1 + \sigma)q_2)/(1 - \zeta) + \sigma)a_0 - 4\dot{a}_0 \sin \pi x \sin \pi z \\ 4\pi^2 \partial C_0 / \partial t - \partial^2 C_0 / \partial z^2 + \pi(a_0 + 4\dot{a}_0) \cos \pi x \sin \pi z \\ \pi(a_0 + 4\dot{a}_0/\zeta) \sin \pi x \cos \pi z \end{pmatrix} \quad (\text{A.13})$$

has a solution if $r_2 = \zeta(1 + \sigma)q_2/(\sigma + \zeta)$; C_0 must decay to zero as there are no x -independent terms to drive it. The solution at this order is

$$\begin{pmatrix} \Psi_2 \\ \theta_2 \\ A_2 \end{pmatrix} = \begin{pmatrix} a_2(t) \sin \pi x \sin \pi z \\ ((a_2(t) - (a_0 + 4\dot{a}_0))/\pi) \cos \pi x \sin \pi z + C_2(z, t) \\ ((a_2(t) - (a_0 + 4\dot{a}_0/\zeta))/\zeta \pi) \sin \pi x \cos \pi z \end{pmatrix}, \quad (\text{A.14})$$

where $a_2(t)$ and $C_2(z, t)$ are as yet undetermined functions.

At third order, the nonlinear terms start to appear:

$$\mathcal{L} \begin{pmatrix} \Psi_3 \\ \theta_3 \\ A_3 \end{pmatrix} = \begin{pmatrix} 0 \\ 4\pi^2 \partial C_1 / \partial t - \partial^2 C_1 / \partial z^2 + (\pi a_0^2 / 2) \sin 2\pi z \\ -(\pi a_0^2 / 2\zeta) \sin 2\pi x \end{pmatrix}. \quad (\text{A.15})$$

No $\sin \pi x \sin \pi z$ term is necessary at this order, but now C_1 is forced by the $\sin 2\pi z$ term; the equation is solved by writing

$$C_1 = -\frac{1}{\pi} c_1(t) \sin 2\pi z, \quad \text{with} \quad \dot{c}_1 = -c_1 + a_0^2/8. \quad (\text{A.16})$$

The solution at third order is

$$\begin{pmatrix} \Psi_3 \\ \theta_3 \\ A_3 \end{pmatrix} = \begin{pmatrix} 0 \\ C_3(z, t) \\ (a_0^2/8\pi\zeta^2) \sin 2\pi x \end{pmatrix}, \quad (\text{A.17})$$

where $C_3(z, t)$ is an as yet undetermined function. At fourth order, the equation

$$\mathcal{L} \begin{pmatrix} \Psi_4 \\ \theta_4 \\ A_4 \end{pmatrix} = \begin{pmatrix} \pi^4 (((\sigma + \zeta)r_4 - \zeta(1 + \sigma)q_4 - \sigma(1 - \zeta)a_0)/(1 - \zeta) + 4(2 + (1 + \sigma)q_2)\dot{a}_0 + \sigma a_2 - 4\dot{a}_2) \sin \pi x \sin \pi z \\ 4\pi^2 \partial C_2 / \partial t - \partial^2 C_2 / \partial z^2 - \pi a_0 c_1 \cos \pi x \sin 3\pi z \\ + \pi(4(\dot{a}_2 - 2\dot{a}_0 - 4\ddot{a}_0) - a_0 + a_2 + a_0 c_1) \cos \pi x \sin \pi z \\ \pi(a_2 - 4\dot{a}_2/\zeta - a_0 - 8\dot{a}_0/\zeta - 16\ddot{a}_0/\zeta^2) \sin \pi x \cos \pi z \end{pmatrix} \quad (\text{A.18})$$

is solved by writing $C_2 = 0$ and

$$\ddot{a}_0 = \kappa \dot{a}_0 - \lambda a_0 - S a_0 c_1, \quad (\text{A.19})$$

where

$$S = \frac{\zeta(\sigma + \zeta)}{16(1 + \sigma + \zeta)(1 - \zeta)}, \quad (\text{A.20})$$

and

$$r_2 = \frac{4(1 + \sigma + \zeta)}{\sigma + \zeta} \kappa, \quad q_2 = \frac{4(1 + \sigma + \zeta)}{\zeta(1 + \sigma)} \kappa, \quad (\text{A.21})$$

$$r_4 = \frac{\zeta^2(1 + \sigma)q_4 - 16\lambda(1 - \zeta)(1 + \sigma + \zeta)}{\zeta(\sigma + \zeta)}. \quad (\text{A.22})$$

In these expressions, the parameter q_4 is specified by higher-order terms. If only the leading-order model (2.10) is required, the choice $q_4 = 16\lambda/\zeta^2$ is convenient as the bifurcations from the trivial solutions of the PDEs (2.1)–(2.4) and the final ODEs coincide exactly: the pitchfork bifurcation occurs when $\lambda = 0$ and the Hopf bifurcation from the trivial solution occurs when $\kappa = 0$ and $\lambda \geq 0$. Equations (A.16) and (A.19) are the ODE model (2.10) to within a rescaling of the variables.

In order to compute the corrections to the ODEs (A.16) and (A.19), it is necessary to go to fifth and sixth order. The equations at fifth order are solved by writing

$$C_3 = -\frac{1}{\pi} c_3(t) \sin 2\pi z, \quad \text{with} \quad \dot{c}_3 = -c_3 + a_0 a_2/4 - a_0 \dot{a}_0/2 - a_0^2/8. \quad (\text{A.23})$$

At sixth order, a second-order ODE for a_2 is obtained. By this stage, the harmonics that appear in the expressions for Ψ_6 , θ_6 and A_6 are the (1,1), (0,2), (2,0), (1,3) and (3,1) modes.

The two second-order ODEs for a_0 (A.19) and for a_2 and the two first-order ODEs for c_1 (A.16) and for c_3 (A.23) may be combined to give a corrected ODE model. Writing

$$v = \sqrt{\frac{S}{8}}(a_0 + L^2 a_2) \quad \text{and} \quad w = S(c_1 + L^2 c_3), \quad (\text{A.24})$$

and choosing

$$r_4 = 16\lambda - 4 \frac{\kappa(1 + \sigma + \zeta - 4\kappa)}{(\sigma + \zeta)}, \quad r_6 = -32\lambda - 64 \frac{\kappa\lambda(1 - \zeta)}{\zeta(\sigma + \zeta)}, \quad (\text{A.25})$$

$$q_4 = \frac{16\lambda}{\zeta^2} - 4 \frac{\kappa(1 + \sigma + \zeta - 4\kappa)}{\zeta(1 + \sigma)}, \quad q_6 = -32 \frac{\lambda}{\zeta^2}, \quad (\text{A.26})$$

in order to eliminate linear terms at order L^2 , the corrected ODEs (2.11) are obtained:

$$\begin{aligned} \ddot{v} &= \kappa \dot{v} - \lambda v - vw + L^2(M_1 \dot{v}w + M_2 vw + M_3 v^3) + \mathcal{O}(L^4), \\ \dot{w} &= -w + v^2 - L^2(v^2 + 4v\dot{v}) + \mathcal{O}(L^4), \end{aligned} \quad (\text{A.27})$$

where

$$M_1 = -4 \frac{(1 + \sigma)}{\zeta(1 + \sigma + \zeta)}, \quad (\text{A.28})$$

$$M_2 = -4\kappa \frac{1 + \sigma + \zeta + (\sigma + \zeta)^2}{(1 + \sigma + \zeta)(\sigma + \zeta)} + 4 \frac{1 + \sigma}{\zeta(1 + \sigma + \zeta)} - 2, \quad (\text{A.29})$$

$$M_3 = -2 \frac{(1 + 3\sigma + 3\zeta)(1 + \sigma)}{\zeta(1 + \sigma + \zeta)(\sigma + \zeta)}. \quad (\text{A.30})$$

The leading-order terms in these corrected ODEs comprise the model (2.10) discussed in the main body of the paper. The parameters R and Q in the PDEs are calculated from κ and λ using (A.1); conversely, κ and λ can be found uniquely from R and Q when L is small by inverting (A.1) and requiring that they be of order one. Using the scaled variables v and w , the first few terms in the asymptotic series for Ψ , θ and A are:

$$\begin{aligned} \Psi &= L^2 \sqrt{\frac{8}{S}} v(t) \sin \pi x \sin \pi z \\ &\quad + 2L^6 \sqrt{\frac{8}{S}} \frac{(1 + \sigma + \zeta)(1 - \zeta)}{\zeta^2(1 + \sigma)} v(t) w(t) \sin \pi x \sin 3\pi z + \mathcal{O}(L^8) \end{aligned} \quad (\text{A.31})$$

$$\begin{aligned} \theta &= L^3 \sqrt{\frac{8}{S}} \frac{v(t)}{\pi} \cos \pi x \sin \pi z - L^4 \frac{16(1 + \sigma + \zeta)(1 - \zeta)}{\pi \zeta(1 + \sigma)} w(t) \sin 2\pi z \\ &\quad - L^5 \sqrt{\frac{8}{S}} \frac{v + 4\dot{v}}{\pi} \cos \pi x \sin \pi z + \mathcal{O}(L^7), \end{aligned} \quad (\text{A.32})$$

$$\begin{aligned} A &= L^4 \sqrt{\frac{8}{S}} \frac{v(t)}{\pi \zeta} \sin \pi x \cos \pi z - L^6 \sqrt{\frac{8}{S}} \frac{v + 4\dot{v}/\zeta}{\pi \zeta} \sin \pi x \cos \pi z \\ &\quad - L^7 \frac{16(1 + \sigma + \zeta)(1 - \zeta)}{\pi \zeta^3(\sigma + \zeta)} v^2 \sin 2\pi x + \mathcal{O}(L^8). \end{aligned} \quad (\text{A.33})$$

Thus solutions to the model ODEs (2.10) provide asymptotically correct solutions to the PDEs (2.1)–(2.4).

The calculation in this Appendix was performed with the aid of the symbolic algebra package Reduce (Hearne 1991).

References

- Arnéodo A, Coulet P H and Spiegel E A 1982 Chaos in a finite macroscopic system *Phys. Lett.* **92A** 369–373
- Arnéodo A, Coulet P H and Spiegel E A 1985a The dynamics of triple convection *Geophys. Astrophys. Fluid Dynamics* **31** 1–48
- Arnéodo A, Coulet P H, Spiegel E A and Tresser C 1985b Asymptotic chaos *Physica* **14D** 327–347
- Arnéodo A and Thual O 1985 Direct numerical simulations of a triple convection problem versus normal form predictions *Phys. Lett.* **109A** 367–373
- Arnol'd V I 1977 Loss of stability of self-oscillations close to resonance and versal deformations of equivariant vector fields (in Russian) *Funct. Anal. Applic.* **11** 1–10
- Bader G and Deuffhard P 1983 A semi-implicit mid-point rule for stiff systems of ordinary differential equations *Numer. Math.* **41** 373–398

- Bykov V V 1978 On the structure of the neighbourhood of the separatrix contour with a saddle-focus (in Russian) *Methods of Qualitative Theory of Differential Equations* Gorky State University, 3–32
- Bykov V V 1993 The bifurcations of separatrix contours and chaos *Physica* **62D** 290–299
- Bykov V V and Shil'nikov A L 1992 On the boundaries of the existence of the Lorenz attractor *Selecta Math. Sov.* **11** 375–382
- Clune T and Knobloch E 1994 Pattern selection in three-dimensional magnetoconvection *Physica* **74D** 151–176
- Coullet P H and Spiegel E A 1983 Amplitude equations for systems with competing instabilities *SIAM J. Appl. Math.* **43** 776–821
- Dangelmayr G, Armbruster D and Neveling M 1985 A codimension three bifurcation for the laser with saturable absorber *Z. Phys. B - Condensed Matter* **59** 365–370
- Dangelmayr G and Knobloch E 1986 Interaction between standing and travelling waves and steady states in magnetoconvection *Phys. Lett.* **117A** 394–398
- Doedel E and Kernévez J 1986 *AUTO: Software for Continuation and Bifurcation Problems in Ordinary Differential Equations* (Pasadena: CalTech Press)
- Freire E, Rodríguez-Luis A J, Gamero E and Ponce E 1993 A case study for homoclinic chaos in an autonomous electric circuit *Physica* **62D** 230–253
- Gambaudo J M, Glendinning P and Tresser C 1992 The gluing bifurcation II: generic unfoldings (in preparation)
- Glendinning P A 1985 Homoclinic bifurcations *PhD dissertation* Cambridge
- Glendinning P A 1988 Global bifurcations in flows *New Directions in Dynamical Systems* ed Bedford T and Swift J (Cambridge: Cambridge University Press) pp 120–149
- Glendinning P and Sparrow C 1984 Local and global behaviour near homoclinic orbits *J. Stat. Phys.* **35** 645–696
- Glendinning P and Sparrow C 1986 T-points: a codimension two heteroclinic bifurcation *J. Stat. Phys.* **43** 479–488
- Glendinning P and Sparrow C 1993 Prime and renormalizable kneading invariants and the dynamics of expanding Lorenz maps *Physica* **62D** 22–50
- Gonchenko S V, Shil'nikov L P and Turaev D V 1993 On models with non-rough homoclinic Poincaré curves *Physica* **62D** 1–14
- Guckenheimer J and Holmes P 1983 *Nonlinear Oscillations, Dynamical Systems and Bifurcations of Vector Fields* (New York: Springer)
- Healey J J, Broomhead D S, Cliffe K A, Jones R and Mullin T 1991 The origins of chaos in a modified Van der Pol oscillator *Physica* **48D** 322–339
- Hearne A C 1991 *Reduce User's Manual - Version 3.4* (Santa Monica: Rand)
- Hughes D W and Proctor M R E 1990 A low-order model of the shear instability of convection: chaos and the effect of noise *Nonlinearity* **3** 127–153
- Knobloch E and Proctor M R E 1981 Nonlinear periodic convection in double-diffusive systems *J. Fluid Mech.* **108** 291–316
- Knobloch E and Weiss N O 1983 Bifurcations in a model of magnetoconvection *Physica* **9D** 379–407
- Knobloch E, Weiss N O and Da Costa L N 1981 Oscillatory and steady convection in a magnetic field *J. Fluid Mech.* **113** 153–186
- Knobloch E, Moore D R, Toomre J and Weiss N O 1986 Transitions to chaos in two-dimensional double-diffusive convection *J. Fluid Mech.* **166** 409–448
- Knobloch E, Proctor M R E and Weiss N O 1992 Heteroclinic bifurcations in a simple model of double-diffusive convection *J. Fluid Mech.* **239** 273–292
- Lorenz E N 1963 Deterministic nonperiodic flow *J. Atmos. Sci.* **20** 130–141
- Lyubimov D V and Byelousova S L 1993 Onset of homoclinic chaos due to degeneracy in the spectrum of the saddle *Physica* **62D** 317–322
- Lyubimov D V and Zaks M A 1983 Two mechanisms of the transition to chaos in finite-dimensional models of convection *Physica* **9D** 52–64
- Malkus W V R and Veronis G 1958 Finite amplitude cellular convection *J. Fluid Mech.* **4** 225–260
- Matthews P C, Proctor M R E, Rucklidge A M and Weiss N O 1993 Pulsating waves in nonlinear magnetoconvection *Phys. Lett. A* **183** 69–75
- Matthews P C and Rucklidge A M 1993 Travelling and standing waves in magnetoconvection *Proc. R. Soc. Lond. A* **441** 649–658

- Moore D R and Weiss N O 1973 Two-dimensional Rayleigh–Bénard convection *J. Fluid Mech.* **58** 289–312
- Nagata M, Proctor M R E and Weiss N O 1990 Transitions to asymmetry in magnetoconvection *Geophys. Astrophys. Fluid Dynamics* **51** 211–241
- Press W H, Flannery B P, Teukolsky S A and Vetterling W T 1986 *Numerical Recipes – the Art of Scientific Computing* (Cambridge: Cambridge University Press)
- Proctor M R E 1992 Magnetoconvection *Sunspots: Theory and Observations* ed Thomas J H and Weiss N O (Dordrecht: Kluwer) pp 221–241
- Proctor M R E and Hughes D W 1991 The false Hopf bifurcation and noise sensitivity in bifurcations with symmetry *Eur. J. Mech. B* **10** 81–86
- Proctor M R E and Weiss N O 1982 Magnetoconvection *Rep. Prog. Phys.* **45** 1317–1379
- Proctor M R E and Weiss N O 1990 Normal forms and chaos in thermosolutal convection *Nonlinearity* **3** 619–637
- Robinson C 1981 Differentiability of the stable foliation for the model Lorenz equations *Dynamical Systems and Turbulence* ed Rand D A and Young L S (Berlin: Springer) pp 302–315
- Robinson C 1989 Homoclinic bifurcation to a transitive attractor of Lorenz type *Nonlinearity* **2** 495–518
- Robinson C 1992 Homoclinic bifurcation to a transitive attractor of Lorenz type, II *SIAM J. Math. Anal.* **23** 1255–1268
- Rodríguez-Luis A J, Freire E and Ponce E 1991 On a codimension 3 bifurcation arising in an autonomous electronic circuit *International Series of Numerical Mathematics* **97** 301–306
- Rucklidge A M 1992 Chaos in models of double convection *J. Fluid Mech.* **237** 209–229
- Rucklidge A M 1993 Chaos in a low-order model of magnetoconvection *Physica* **62D** 323–337
- Rucklidge A M and Matthews P C 1993 Shearing instabilities in magnetoconvection *Solar and Planetary Dynamos* ed Proctor M R E, Matthews P C and Rucklidge A M (Cambridge: Cambridge University Press) pp 257–264
- Rucklidge A M and Matthews P C 1995 Analysis of the shearing instability in nonlinear magnetoconvection (in preparation)
- Rucklidge A M, Weiss N O, Brownjohn D P and Proctor M R E 1993 Oscillations and secondary bifurcations in nonlinear magnetoconvection *Geophys. Astrophys. Fluid Dynamics* **68** 133–150
- Shil'nikov A L 1986 Bifurcations and chaos in the Morioka–Shimizu system (in Russian) *Methods of Qualitative Theory of Differential Equations* Gorky State University, 180–193. Published in English (1991) *Selecta Math. Sov.* **10** 105–117
- Shil'nikov A L 1989 Bifurcations and chaos in the Morioka–Shimizu model: II (in Russian) *Methods of Qualitative Theory of Differential Equations and Theory of Bifurcations* Gorky State University, 130–138
- Shil'nikov A L 1993 On bifurcations of the Lorenz attractor in the Morioka–Shimizu model *Physica* **62D** 339–346
- Shil'nikov A L, Shil'nikov L P and Turaev D V 1993 Normal forms and Lorenz attractors *Int. J. Bifurcation and Chaos* **3** 1123–1139
- Shil'nikov L P 1965 A case of the existence of a countable number of periodic motions *Soviet Math. Dokl.* **6** 163–167
- Shimizu T and Morioka N 1980 On the bifurcation of a symmetric limit cycle to an asymmetric one in a simple model *Phys. Lett.* **76A** 201–204
- Sparrow C 1982 *The Lorenz Equations: Bifurcations, Chaos, and Strange Attractors* (New York: Springer)
- Takens F 1974 Forced oscillations and bifurcations *Comm. Math. Inst., Rijksuniversiteit Utrecht* **3** 1–59
- Veronis G 1966 Large-amplitude Bénard convection *J. Fluid Mech.* **26** 49–68
- Weiss N O 1981 Convection in an imposed magnetic field. Part 1. The development of nonlinear convection *J. Fluid Mech.* **108** 247–272
- Weiss N O 1991 Magnetoconvection *Geophys. Astrophys. Fluid Dynamics* **62** 229–247